Design Optimization and Field Performance Evaluation of the Wave Suppression and Sediment Collection (WSSC) System: Computational Fluid Dynamics (CFD) Modeling, Surface Elevation Table (SET) Survey, and Marker Clay Study

A Thesis

Presented to the

Graduate Faculty of the

University of Louisiana at Lafayette

In Partial Fulfillment of the

Requirements for the Degree

Master of Science

Salman Sakib

Summer 2017

Design Optimization and Field Performance Evaluation of the Wave Suppression and Sediment Collection (WSSC) System: Computational Fluid Dynamics (CFD) Modeling, Surface Elevation Table (SET) Survey, and Marker Clay Study

Salman Sakib

APPROVED:

Daniel Gang, Chair Professor of Civil Engineering	Kenneth McMannis Professor and Head of Civil Engineering
Peng Yin Assistant Professor of Mechanical Engineering	Jenneke Visser Professor of Geosciences
Mary Farmer-Kaiser Dean of the Graduate School	

DEDICATION

Dedicated to my parents Md Jamilur Rahman and Sultana Ruksana Parvin, who always supported me in every endeavor of my life.

ACKNOWLEDGMENTS

I would like to thank Dr. Daniel Gang for keeping his faith in me and for supporting me throughout my graduate studies at the University of Louisiana at Lafayette. Without his guidance, this journey would never have been possible. I owe a lot to my previous research partner Grant Besse, who not only brought me up to speed in our research project with patience but also helped me settle into a new city like Lafayette.

I would also like to thank Dr. Kenneth McManis, Dr. Peng Yin, and Dr. Jenneke Visser, who graciously served on my thesis committee. In addition, I would like to express my gratitude to Mark LeBlanc, Sharon Hall, Dr. Donald Hayes, Andre Daugereaux, Dr. Elman Bashar, Nusrat Jahan, Zaki Uddin Ahmad, Jonathan Trahan, Syed Ahnaf Morshed, Monjurul Islam Rifat, Sakib Mahmud, Md Reshad Reza, A B M Tanvir Pasha, Sabbir Billah Mishu, Qiyu Lian, Mas Konggidinata, and the Civil Engineering faculty for their help throughout my time conducting research.

Special thanks to my family and loved ones whose friendship and support throughout my life have allowed me to earn my degrees and complete my thesis. Lastly, I would like to thank all those special persons who showed me unconditional love and care through joyful and rough times at the University of Louisiana at Lafayette.

TABLE OF CONTENTS

LIST OF FIGURES

LIST OF TABLES

LIST OF EQUATIONS

CHAPTER 1: INTRODUCTION

An estimated three billion people or nearly half of the world's population live within 200 km of coastlines (Creel, 2003). This fact highlights the importance and urgency of addressing the global issue of protecting coastal regions. Coastal areas provide enormous economic opportunities for the massive population living in those regions. These benefits include food production from fisheries, tourism, fishing and recreational hunting, and connectivity for sea transportation. In addition, coastal regions are an important source of acquiring industry resources, such as water, large lands, and access to ports. Around 50% of the world's wetlands and 20% of the world's mangroves have been lost during the 20th century (Creel, 2003). The importance of coastal wetlands can be observed from the fact that they act as a protective and self-sustaining buffer against storms, especially hurricanes and tropical storms (Smith, 1993). According to the estimates, coastal wetlands in the U.S. provide protective cover worth $23.2 billion. There are numerous other benefits, but these are the most important reasons for protecting coastal wetlands for the benefit of the society (Costanza et al., 2008).

Coastal wetlands are an important part of Louisiana's economy and its culture and heritage (Keddy, 2008). The rate of coastal wetland loss in Louisiana is alarming and has exceeded over 40 square miles per year in the last fifty years (Louisiana Coastal Wetlands Conservation and Restoration Task Force, 1998). Since the 1990s, the total coastal wetland loss in Louisiana alone is estimated to be in the range of 25 to 35 square miles per year. Wetland loss in Louisiana alone amounts to 80% of the total wetland loss in the U.S. every year (Tibbets, 2006). This loss of coastal wetlands has substantial impacts on the economy and culture of the region. It adversely affects many areas such as commercial fishing and trapping, water quality, recreational hunting and fishing, storm surge buffering, and flood control. Overall, the disappearance of these wetlands will

cause an estimated loss of $37 billion by the year 2050 (Louisiana Coastal Wetlands Conservation and Restoration Task Force, 1998).

Mitigating and reducing the effect of wetland loss is of prime importance throughout the world. Conservation and upkeep of shorelines are the goals of many coastal protection programs. Building hard structures for the protection of coastal regions has been in practice for many years (Piazza et al., 2005). Construction of hard structures alters the sediment balance as it disrupts the flow of sediment in the area (Birben et al., 2007). Vegetative planting and oyster reef creation have emerged as alternatives to the standard hard shoreline protection methods.

Porous breakwaters have long been studied and used to protect shorelines from further erosion (Huang and Chao, 1992). By reducing the energy of waves, these structures promote sedimentation of littoral material in the protected area behind the structure (Birben et al., 2007). It is a unique challenge to protect coastal wetlands where the aquatic substrate is typically very soft, highly organic, and susceptible to erosion. Conventional shoreline protection structures are costly in these environments, and many coastal structures are too heavy to be supported by the soft foundation materials. A viable alternative is needed to slow and possibly reverse the trend of coastal erosion.

A new alternative to rock breakwater systems was created by Pierce Industries, LLC of Cut Off, Louisiana. It is an innovative shoreline protection device as shown in Figure 1, called the Wave Suppression and Sediment Collection System (WSSC) or Wave Robber™, with patent Publication Number of EP246192B1. The device has a slope in the front with steps projecting itself perpendicular to the openings on the face. These openings have pipes fitted to connect the front face with the back. The pipes slant downward to ensure that sediment-laden water slides toward the rear part and

accumulates there. Also, to prevent the backflow of the water, check valves are placed at the back of the pipes.

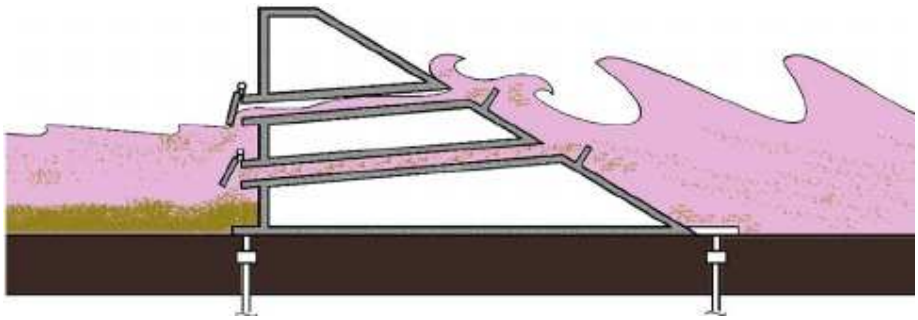

Figure 1: WSSC System (Image Credit: Pierce Industries, LLC)

Accurately forecasting a structure's performance is the most difficult task while designing coastal structures (McCormick, 1993). Accurate models for predicting the shoreline's response to the coastal structures are vital in designing those structures (Kristensen et al., 2013). Areas surrounding the coastal protection structures may face issues such as erosion due to improper prediction from the models (McCormick, 1993). The performance of these structures is usually evaluated and validated through physical modeling. Physical modeling has limitations in terms of construction time and equipment availability (Jacobsen et al., 2015). With advances in computational techniques, Computational Fluid Dynamics (CFD) has become a cheaper and more practical alternative when compared to physical modeling of shoreline protection structures (Cavallaro et al., 2012).

Previous studies have evaluated the WSSC units' performance in the laboratory setting. McCoy (2015) investigated the laboratory silt-clay transport efficiency of the technology along with wave reduction potential. Besse (2016) studied the laboratory performance of the units in terms of sand sediment transport, hydrodynamic efficiencies, and wave reduction modeling using computational fluid dynamics (CFD) tools. The units' sediment transport phenomenon has never been modeled using CFD tools for

design optimization to yield maximum wave reduction and sediment transport benefits. The primary objectives of this study are:

- To assess the sediment collection efficiency of various models using the computational fluid dynamics (CFD) tool Ansys FLUENT.
- To optimize different parameters of the WSSC units for optimizing energy dissipation and sediment accumulation.
- To investigate the units' application feasibility in a real-world scenario using field investigations. The field site investigation involved real WSSC units and their performance in stopping coastal erosion. The sediment accretion data were gathered using Surface Elevation Tables (SET) and marker clay experiments.

CFD modeling technique used in this study can be used as a valuable tool to assess the performance of the WSSC devices, as well as for other shoreline protection devices. In order to determine the effect of face slope and pipe diameters on the efficiency of sand collection, multiple geometries of WSSC technology were modeled using different experimental conditions. The models' performance was studied in terms of sediment transport behind the units. Ansys FLUENT, well-known CFD software, was used for parametric optimization.

Field investigation will assess the WSSC technology's performance in low-energy areas such as Louisiana coastal marshes and wetlands. SET data will be collected over a year to see if the technology is able to stop coastal erosion and at the same time build more lands. Marker clay experiments will be conducted to validate the SET accretion data.

CHAPTER 2: COASTAL EROSION AND RESTORATION TECHNIQUES

2.1 Louisiana's Coast

The environment of deltaic plains is dynamic in nature and keeps changing over time. The Louisiana coast has seen a continuous change for the past millions of years. The Mississippi river, one of the major rivers of North America, keeps changing its path and creates natural divisions or overlapping lobes in the deltaic plains that are bounded by embankments and natural levee ridges (DeLaune et al., 1992, Kolb and Van Lopik, 1996). Floods on the Mississippi's natural levees every year have resulted in the formation of large swathes of marshlands (DeLaune et al., 1992). A large deltaic plain of the Mississippi has formed over time because of more land accumulation as compared to erosion (Fraizer, 1967). At the present time, land loss in Louisiana is exceptional as compared to all other coastal areas of the United States (Georgiou et al., 2005).

Coastal marshes are extremely important for the Louisiana coast and provide many benefits to the region such as storm protection and habitats for different types of wildlife. In addition, these marshes are vital to sustaining the population's way of life. A large part of Louisiana's population lives near the coast, and much of the economy involved in hunting and fishing is dependent on these marshes (Coreil, 1995).

The Mississippi river used to change its course every 1000 – 2000 years and formed new delta lobes, thus replacing the older deteriorated delta lobes. In recent times, this process was restricted, with increased human interactions forcing the river down its current path. At present, the sediments are deposited onto the continental shelf instead of being deposited towards the Atchafalaya River (DeLaune et al., 1992). The amount of suspended sediment load deposited onto the continental shelf (DeLaune, et al., 1992) is approximately 21200 metric tons (Meade and Parker, 1985). Two primary factors

contributing to wetland loss in Louisiana are offshore deposition of sediments and subsidence (Salinas et al., 1986).

2.2 Land Loss

Coastal land loss is a widely-studied topic due to its complex nature, and many have made progress towards the conservation of marshes and wetlands (Morang et al., 2012). The natural process of sediments being deposited along the surrounding marshes and wetlands has been disturbed, since the 1920s, by the human activity of installing levees along the Mississippi River. This disruption caused by human activities has severely affected the natural sediment deposition cycle, which is one of the major reasons for coastal wetland loss within Mississippi River delta (Salinas et al., 1986).

2.2.1 Subsidence

The main factor of wetlands loss is the subsidence. There are many factors determining wetland loss, including consolidation of recently deposited sediments; changes in sedimentation patterns; and underground fluid withdrawal (Salinas et al., 1986; Day et al., 2000). Within Louisiana's coastal plains, the highly organic sediments are extremely impacted by primary and secondary consolidation. The rate of subsidence is higher because of sediments being subjected to these processes immediately after deposition (Walker et al., 1987).

2.2.2 Erosion

Coastal communities around the world are concerned about the issue of coastal land loss and conversion of wetlands to open water. Erosion along the shoreline is one of the major factors that contributes towards the conversion of wetlands to open water (Huang and Chao, 1992). Erosion is the process of sediments being removed by wave action and is very different from inundation, which is submergence of land due to rise in sea level (Nicholls et al., 1995). The seriousness of this issue can be imagined from the

fact that Louisiana's wetland loss amounts to 80 % of the total occurring in the nation, while the state contains about 40 % of the United States' coastal wetland (Penland and Ramsey, 1990).

2.3 Current Erosion Control Methods

Protecting our coastal areas is a high priority around the world. The prime focus of many coastal protection programs is to maintain and sustain the integrity of the shorelines. Hard and non-sustainable materials have been used to protect the shorelines but they are not natural to the very ecosystem they protect (Piazza et al., 2005).

2.3.1 Hard Structures

Hard structures such as breakwaters are used worldwide to protect the shorelines. These structures have multiple engineering applications, such as preventing erosion of beaches; reclamation of shoreline through the accumulation of sediments on the shoreline; effectively protecting water bodies from offshore wave action; and preventing silting of the harbor entrance. To achieve these four goals, breakwaters are designed in such a way to reduce the height of waves in the target areas. In most instances, this is mainly due to wave diffraction (Rosen, 1982).

2.3.1.1 Breakwaters

In coastal and ocean engineering, porous breakwaters have been studied for a long time (Huang and Chao, 1992). Disconnected porous breakwaters have been widely used to protect shorelines (Yu, 1995). These structures reduce the energy of the waves and allow accumulation of sediments behind the structure (Birben et al., 2007).

Sediment deposition is encouraged on the shoreward side of the structure where wave energy is in a reduced state. Littoral sediment material accumulates, and less sediment is lost in this protected area behind the breakwater. This sediment accumulation generally appears as a spit of sand emerging from the beach towards the breakwater,

known as a salient, or a tombolo if the salient connects to the breakwater (Birben et al., 2007).

Two ways of constructing offshore breakwaters are as a single unit or as a series of units. While a single breakwater may be used to protect a small area and has limited effect on the overall shoreline current profile, multiple units may be constructed to aid in the reclamation of a longer stretch of coast. These systems of multiple breakwaters, or segmented breakwater systems, are designed with specified design widths and spacing (Birben et al., 2007).

2.3.1.2 Groynes

Groynes are hard structures built at the right angles to the shoreline to retain the sand on the shore and prevent erosion. There can be many groyne structures erected across the shoreline to retain the sand on the coast. Their purpose is to hold the sand on the beach and reduce the impact of waves in the inner surf zone (Van Rijn, 2011). The updrift end on the groyne accumulates sediments and the downdrift of the groyne structure experiences sediment deficit, which leads to erosion (Nersian et al., 1992). Fleming (1990), Kraus et al. (1994), U.S. Army Corps of Engineers (1994), and Van Rijn (1998, 2005) have also given general overviews on groynes.

2.3.2 Other Alternatives

The hard structures, such as groynes, jetties, breakwaters, etc., are built to protect the shoreline from erosion by disrupting the flow patterns in surrounding regions and thus changing the sediment balance (Birben et al., 2007). These adverse effects of hard structures have increased the need to find alternative solutions for protecting the shorelines. As a result, the coastal engineering community has been experimenting with comparatively non-intrusive “living shoreline” protection strategies (Seyphers et al., 2011).

2.3.2.1 Vegetative Planting

Coastal wetlands have been known to provide benefits such as shoreline stabilization and coastal protection. According to the research done for many years, vegetation along the shores such as marsh vegetation and mangroves has been effective in providing protection against storms and erosion (Gedan et al., 2011).

Coastal vegetation not only protects the shoreline from storms and erosion but also provides a habitat for wildlife, improves water quality, and regulates water levels. Root systems of vegetation also help in stabilizing both shorelines and dune systems (Augustin et al., 2009). Shepard et al. (2011) conducted a systematic literature review on the benefits of salt marshes. Their analysis included studies on wave attenuation, shoreline stabilization, and floodwater attenuation of coastal marshes. All seven studies included in the meta-analysis found that areas with vegetation had a significant effect on wave attenuation when compared to non-vegetated areas. Attenuations from these studies ranged between wave reductions of 52±24% on average. It was found that higher transect lengths resulted in more reduction in wave energy affecting the shoreline. Other factors that were found to reduce the impact of waves are vegetation density, vegetation stiffness, and marsh width. Factors such as vegetation species type, vegetation density, vegetation height, and biomass production are most commonly correlated with shoreline stabilization (Shepard et al., 2011).

2.3.2.2 Oyster Reefs

Oyster reefs are hypothesized to stabilize shorelines by reducing wave energies along the marsh and estuarine shorelines with their coarse structures (Piazza et al., 2005). Meyer et al. (1997) studied the possible value of introducing oyster cultch to the lower intertidal fringe of three created coastal marshes. Significant differences were found between cultched and non-cultched control sites. The areas with oyster cultches were

found to show gradual land accumulation, while non-treated areas had losses (Meyer et al., 1997).

Piazza et al. (2005) studied the effects of oyster reefs created along the edges of eroding marsh shorelines in Louisiana. Test sites were comprised of a location having low and high wave energy. Results showed that shoreline withdrawal was effectively reduced at a location with low wave energy. However, there was no significant benefit of Oyster treatment at the location with high wave energy. Researchers concluded that oyster reefs may be a sustainable method of protecting low-energy areas from shoreline withdrawal (Piazza et al., 2005).

2.3.3 Limitations of Current Methods

- The soil in Louisiana marshes contains a high amount of clay (30-65%) and a large amount of organic matter (Edwards and Proffitt, 2003). These factors make the soil not suitable for hard breakwaters. Kudella et al. (2006) studied pore pressure generation beneath caisson breakwaters on loose sand with thin clay or silt layers. Their study showed that residual pore pressure was generated by the caissons due to breaking wave loads. This residual pressure was closely related to soil deformations and could lead to the failure of the breakwater (Kudella et al., 2006). These soil conditions would require more specialized materials such as geotextiles, in order to build hard structures on marsh soils, and would greatly increase their cost.
- Groynes are heavy and costly to construct and they face the same issues as breakwaters in the marsh setting.
- Vegetative planting is sensitive to temperature, water level, and salinity. A drastic change in any of these factors will disrupt the vegetation set up.

- Oyster reefs are likely to be an effective solution in areas with low wave energy. They are practically ineffective in providing protection for areas with high wave energy. Also, oyster reefs are sensitive to water salinity and in brackish water environment oysters cannot sustain.

2.3.4 Wave Suppression and Sediment Collection System

Current technologies used to protect the shorelines accrue high cost and hence, new, innovative and economical approaches are necessary to protect the shorelines. A possible alternative shoreline protection device is the Wave Suppression and Sediment Collection (WSSC) system. The purpose of the WSSC system is to reduce wave action along shorelines, navigation channels, and canals while retaining sediment behind the units. Some advantages the WSSC system has over current methods are as follows:

- Transporting rock jetties to the areas of interest is difficult. The WSSC units are made of High-Density Polyethylene (HDPE) and are easier to transport.
- These units weigh less compared to the rock structures, reducing the concern for soil failure.
- The units are modular in design and can be moved individually.
- Units are not permanent and can be moved in case the desired shoreline response is obtained or if adjustments need to be made to obtain the desired response.
- This system can be used along with vegetative planting in order to sustain gradual accumulation on the shoreline.

2.4 Computational Fluid Dynamics (CFD) Modeling

In the past, field experience and limited empirical rules were the basis of design and construction of breakwater systems (Rosen, 1982). Recently, computational modeling and laboratory experiments have been used to study the complex phenomenon occurring in the coastal environment. Breakwater characteristics, sediment contribution, wave

properties, and sediment characteristics are some of the variables that play an important role in reducing wave energy and sediment transport (Ming and Chiew, 2000). Inaccurate predictions of shoreline response to a coastal structure may cause undesired erosion in the surrounding areas (McCormick, 1993). This shows that accurate models to predict shoreline response to shoreline protection devices are necessary for the planning and design of these structures (Kristensen et al., 2013).

Physical modeling is often used to validate the performance of the coastal structure (Jacobsen et al., 2015). The amount of time it takes to construct a physical model and the amount and size of the wave tanks limit the current method of physical modeling (Jacobsen et al., 2015). Computational Fluid Dynamics (CFD) is used in many applications in order to reduce costs and time of physical modeling. Over the last ten years, it has become a more feasible method of modeling (Cavallaro et al., 2012). Other authors, such as Higuera et al. (2014), have completed validation of 3D RANS models for porous coastal structures and their results show that CFD could be a valuable tool in assessing the performance of coastal structures. This can be useful in the initial design of coastal structures, where physical models are typically unfeasible and the knowledge extracted from previous designs is lacking (Jacobsen et al., 2015). In order to optimize the technologies, multiple designs of the shoreline protection structures are studied. Advances in the field of computing have enabled the simulation of physical models to reasonable levels of certainty using the computer-modeling software. The time and cost of optimizing a device got greatly reduced with the use of computer modeling alongside physical modeling.

Multiple software programs exist for the function of fluid dynamic modeling. Numerical methods and algorithms used in Computational Fluid Dynamics (CFD) solve fluid flow problems (Anderson and Wendt, 1995). Many different programs have been

developed for solving CFD problems. Some of these CFD programs include FLUENT and OpenFoam. These programs use the same general equations to solve fluid flow problems; mainly Reynolds-averaged Navier-Stokes equations.

Some of the basic equations used by CFD solvers are the following: Instantaneous Continuity Equation (Eq. 1), Momentum Equation (Eq. 2), and the Energy Equation (Eq. 3).

$$\frac{\partial \rho}{\partial t} + \frac{\partial}{\partial x_j}\left[\rho u_j\right] = 0 \qquad \text{(Eq. 1)}$$

$$\frac{\partial}{\partial t}\left(\rho u_i\right) + \frac{\partial}{\partial x_j}\left[\rho u_i u_j + p\delta_{ij} - \tau_{ji}\right] = 0, \quad i = 1,2,3 \qquad \text{(Eq. 2)}$$

$$\frac{\partial}{\partial t}\left(\rho e_0\right) + \frac{\partial}{\partial x_j}\left[\rho u_j e_0 + u_j p + q_j - u_i \tau_{ij}\right] = 0 \qquad \text{(Eq. 3)}$$

There are many benefits of using CFD, including experimental time is generally shortened; designs can be changed and tested with relative ease; it is typically less costly than physical modeling, and multiple designs can be tested at once with CFD software. There are few limitations of using CFD in the design process such as CFD models must first be validated by physical experiments; some highly detailed CFD models may take a long time; 3D CFD models accrue higher computational cost; some aspects of the physical processes may not be currently feasible to model using CFD. Another downside of computer modeling is that numerical simulations must be calibrated based on experimental tests to obtain the best results (Higuera et al., 2014)

2.4.1 Sediment Transport Modeling

The modeling of sediment transport has always been complicated and it requires a sound understanding of topics, such as fluid dynamics, river engineering, and sedimentation. The calculation of sediment settling velocity is a combination of gravity, buoyancy, and drag forces. Many sediment transport studies have been conducted in

which Stokes' Law was used with different assumptions. CFD modeling of sediment transport also involves the effect of particle diameter, fluid turbulence, and flow conditions which are usually defined by researchers for any particular modeling problem.

The complexity of sediment transport with water arrives when sediment particles move under wave actions which require the stable modeling solution of the wave phenomenon as the first step. Flow turbulence, reflection, and moving eddies affect the particle trajectories which can be tracked by stochastic particle tracking approach. Irregular waves create fluctuating sediment settling velocities, which results in nonlinear trends of sediment deposition rates. Thus, modeling of sediment transport through breakwaters requires time-intensive simulation two-phase problems where both wave actions on the breakwater and sediment deposition through the breakwater must be calculated.

In a study conducted by Thinglas and Kaushal (2008), the interaction of particles and fluid for the trap shape design in a sewer was investigated using a 2-D model. The RNG k-ε turbulence model was selected and Lagrangian approach was adopted to track particles in the fluid medium. Boundary conditions for inlet and outlet were defined as velocity-inlet and pressure-outlet, respectively. Boundary behavior for Discrete Phase Model (DPM) was selected as 'trap' and 'reflect' for particles at the outlet region. Results from the 2D model were compared with the 3D model results and it was found that absence of lateral flow did not allow eddies to form. Researchers concluded that 3D simulation was necessary for accurate prediction of the interaction between particles and the structure (Thinglas and Kaushal, 2008).

Tarpagkou and Pantokratoras (2013) also studied the interaction between particles and fluid in a sedimentation tank using Ansys FLUENT. The study investigated the effect of particle size and volume fraction on the flow properties. This study also adopted the

Lagrangian approach and k-ε turbulence model for turbulence modeling in the computational domain. The study used velocity-inlet and pressure-outlet boundary condition and the boundaries were defined as 'escape' to treat the particles in the discrete phase model (DPM). It was concluded from the study results that general influence on fluid phase was impacted positively when particle diameter and volume fraction were higher (Tarpagkou and Pantokratoras, 2013).

In the study by Yan et. al. (2014) a new boundary condition was used to simulate the sedimentation phenomenon in the Djargo Reinhardt basin using Ansys FLUENT as the computational tool. The k-ω turbulence equations were adopted for modeling fluid turbulence in the computational domain. Volume of Fluid (VOF) method was selected for multiphase fluid flow and 20000 particles were introduced into the system using the particle injection function of the discrete phase model (DPM). Velocity-inlet and pressure-outlet boundary conditions were chosen for the fluid flow. A 'user defined function (UDF)' boundary condition was provided into the model for the basin bed which incorporated the combination of the 'trap' and 'reflect' function of boundary conditions. Results from this study indicated that there was variation between experimental data and simulation output caused by the geometrical differences. Threshold Kinetic Energy (TKE) was calculated for the bed boundary condition and it was concluded that UDF can be used to define the particles at the bottom and bed boundary condition (Yan et al., 2014).

CHAPTER 3: METHODOLOGY AND EXPERIMENTAL SETUP

3.1 Computational Fluid Dynamics Model

This chapter focuses on the theoretical background and the properties of the Computational Fluid Dynamics (CFD) software that was used in this study. Different Computational Fluid Dynamics (CFD) packages are available to simulate flow over hydraulic structures. The CFD package should preferably fulfill the following requirements:

- Non-hydrostatic flow calculations
- Possibility to simulate sediment transport
- Advanced turbulence modeling
- Free surface modeling.
- Technical support available
- Limited computation times

After testing different software packages, it was decided that Ansys FLUENT would be used for the numerical simulation of the wave tank for sediment transport modeling. FLUENT is a Computational Fluid Dynamics (CFD) package from the American company Ansys. A brief description of this model is given in this section. For more detailed information, reference is made to the FLUENT User Guide; see FLUENT INC (2005). The content of this section is partly based on this User Guide.

3.1.1 General

FLUENT is capable of simulating both two-dimensional and three-dimensional situations. Both structured and unstructured meshes are possible. Different types of elements are permitted, such as quadrilaterals and triangles for 2D simulations and hexahedra, tetrahedra, polyhedra, prisms, and pyramids for 3D simulations. The geometry, mesh, boundary types, and volume types can be specified in the preprocessor

Ansys Workbench. The Ansys 17.0 student package was used for the numerical study on sediment transport modeling. The model setup in FLUENT is described sequentially in the following sections from geometry preparation, meshing, complete model setup including multiphase flow, turbulence, boundary conditions, wall functions, material properties, discrete phase model, simulation environment, and post-processing of generated data.

3.1.2 Geometry Preparation

The model was prepared in Ansys Workbench 17.0 using a Fluid Flow (Fluent) model as shown below. Geometry preparation is the first step of modeling fluid flow over a hydraulic structure. The geometry of the WSSC units and wave tank was prepared in a two-dimensional plane in the Ansys DesignModeler (DM), as the modeling of the fluid flow and sediment transport was intended to be modeled in a 2-D environment. This task was repeated to test different designs by creating them in DesignModeler and meshing them in the Mesh component.

Figure 2 shows the geometry of the created surfaces in three sections. The wave tank was divided into three sections for the ease of data collection and model setup; each zone of the wave tank is responsible for different fluid phenomena. A thematic diagram of the wave tank with zones is shown below in Figure 3. A step-by-step guide for the geometry preparation can be found in Appendix A.

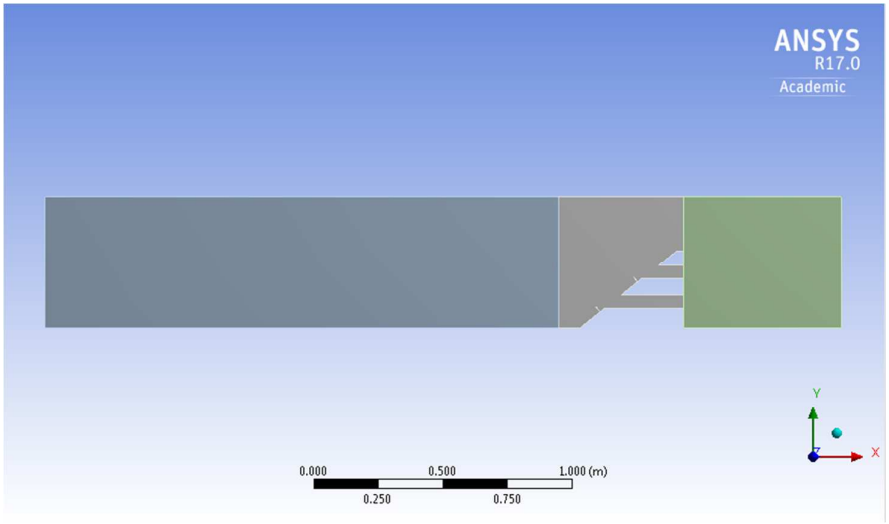

Figure 2: Wave Tank Geometry with Surfaces

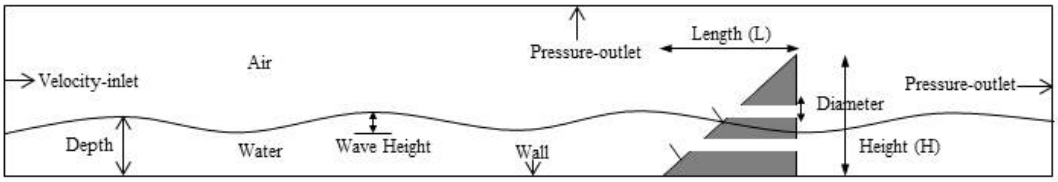

Figure 3: Schematic Diagram of the Wave Tank with Boundary Conditions

3.1.3 Meshing

After preparation of the model geometries they were transferred to the meshing component of the Fluid Flow model automatically. The meshing maximum grid size was selected to be 4.5656e-003 m for computational stability. The curvature of the grids was selected as “Fine” and the minimum grid size was automatically generated from the Meshing component. The different connections of the wave tank were detected and generated for the unobstructed flow of incompressible fluids in the wave tank. Different surfaces of the wave tank were named using the name selection function so that boundary conditions could be properly applied in the model setup. Also, using the same function, the tank zones were named for better data accuracy of sediment concentrations in different tank zones. The surfaces have to be named in the mesh component so that later

those can be used for simulation and generation of results. Figure 4 shows the meshed wave tank with the hydraulic structure ready to be transferred into the FLUENT component for model setup.

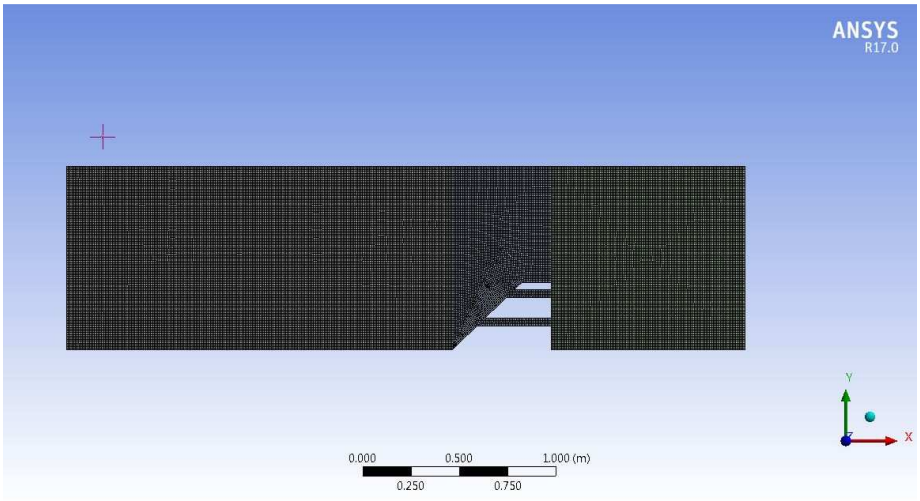

Figure 4: Meshed Wave Tank and WSSC System Geometry

3.1.4 Model Setup

The model setup included many small steps, during which the model was defined using different environmental variables. The Volume of Fluid (VOF) method was chosen for the multiphase flow model. Two Eulerian phases were selected for the fluid flow in the wave tank, with one being air and the other being water. The realizable k-ε (k-epsilon) turbulence model was selected with the standard wall function. Boundary conditions were selected as "velocity-inlet" and "pressure-outlet" for the left and right walls of the tank. The primary fluid phase was selected as "air," and "water" was assigned as the secondary fluid phase in FLUENT. Table 1 summarizes the important input parameters of the sediment transport model.

Table 1: Important Model Input Parameters in FLUENT

Parameter	Values
Gravity	-9.81 (m/s^2)
Particle Density	1.3 (kg/m^3)
Fluid Phases	Air and Water
Operating Pressure	101325 (Pascal)
Operating Density	1.225 (kg/m^3)
Pressure-Velocity Coupling	One Way
Pressure Discretization	PRESTO!
Momentum Discretization	Second Order Upwind
Flow Velocity Magnitude	0.018 (m/s)
Free Surface Level	0.1905 (m)
Wave Height	0.0762 (m)
Wave Length	1.5 (m)
Wave Theory	Second Order Stokes

3.1.5 Simulation Output

Monitors were assigned to the different zones of the wave tank to calculate the volumetric concentration of discrete phase particles (sediment), and the results were saved as output files for post-processing. The post-processing was done in Microsoft Excel, where the graphs on concentration change over time were generated.

3.2 Laboratory Experimental Setup

After the results from the simulation study were generated, the parametric optimization analysis was performed. To investigate and validate the simulation of the proposed WSSC (submerged type) units, experimental studies were carried out in a wave tank (3.83 m long, 1.83 m wide, and 0.508 m deep) at the Hydraulics Laboratory at the University of Louisiana at Lafayette (Besse, 2016). Three units were evaluated in the previous study for sediment collection experiments. Two of these units have the approximately equal open area, allowing this parameter to be directly compared. Figures 5, 6, and 7 show the three different lab-scale models used during the experiments. The

main differences between Unit 1, 2, and 3 are the number of pipes connecting the front and back of the units and the sizes of these pipes. Unit 1 has 72 pipes with a diameter of 1.19 cm and a total area of 205 cm^2. Unit 2 has 10 pipes with a diameter of 5.08 cm and a total area of 202 cm^2. Unit 3 has 6 rectangular slots with a dimension of 20.32 by 5.08 cm (equivalent diameter of 11.46 cm) and a total area of 619 cm^2.

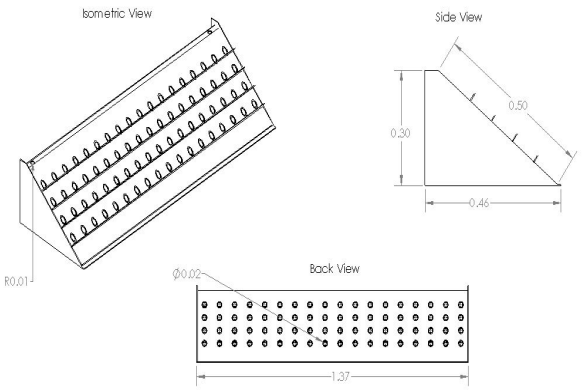

Figure 5: Dimensions of Unit 1 with 1.91 cm Diameter Pipes (McCoy et. al., 2015)

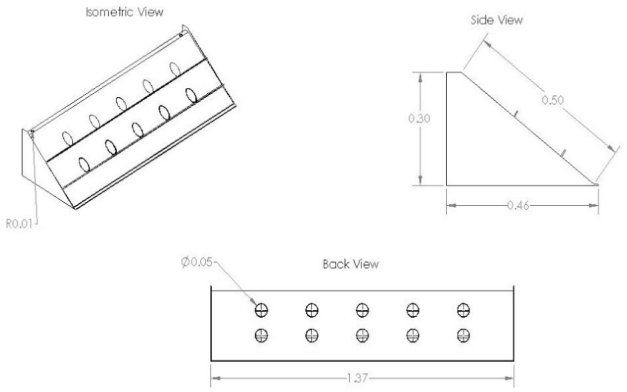

Figure 6: Dimensions of Unit 2 with 5.08 cm Diameter Pipes (McCoy et. al., 2015)

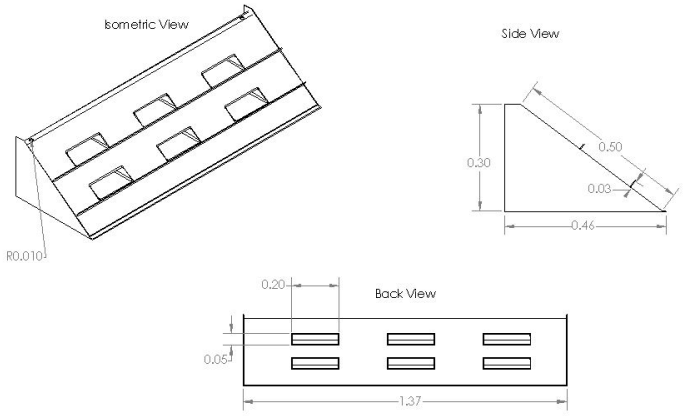

Figure 7: Dimensions of Unit 3 with 5 cm by 20 cm Slots (McCoy et. al., 2015)

The length, width, and height of the units are 1.37 m, 0.46 m, and 0.3 m; they were made of HDPE plastic and were installed in the wave tank containing 0.1905 m still water depth. Regular waves ranging from 0.8 m to 4.0 m were generated from a flap type wave generator installed at the upstream end of the wave tank. The units spanned 90% of the width of the tank, shown in Figure 8 along with the dimensions of the tank. The units were constructed that way for ease of installing and removing them from inside the tank. Units were placed 1.99 m away from the base of the wave paddles. A weir was used beside the units to cover the full width of the tank and to prevent sediment movement through the side. The sealed 0.15 m wide and 0.15 m tall weir was placed behind a 0.30 m tall sheet pile to deflect any waves toward the unit and to prevent the sediment from transferring over the lower weir from the front of the tank. The water depth used in the study was 0.1905 m. The detailed setup can be found in the earlier study conducted on these units (McCoy et al., 2015) and in Figure 8.

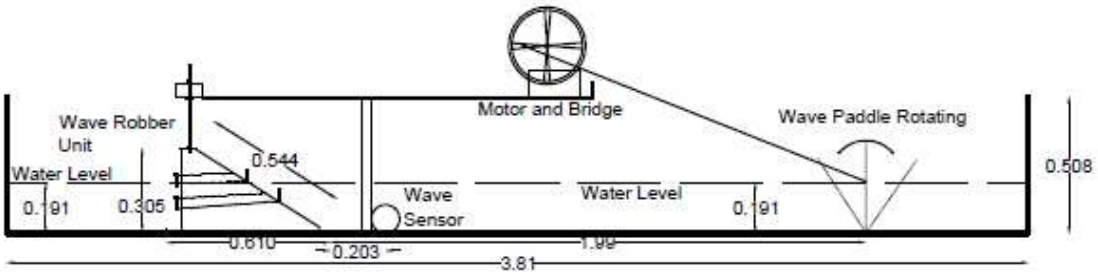

Figure 8: Experimental Setup of the Tank

The units were sealed with Plumber's Putty™ to eliminate flow between the bottom of the unit and the floor of the tank. This also ensured that sediment collected behind the unit was transferred through the pipes of the units. A framing system was used to increase the normal forces acting on the unit, thereby forgoing the need to increase the weight of the unit in order to achieve sufficient friction forces. Two 6.35 cm diameter all-thread rods were used to attach the frame to the units and provided compression forces on either end, which achieved sufficient normal forces to keep the unit in place throughout the experiment. This exact setup was replicated in a CFD model and the results were used to validate the CFD wave reduction data in the previous study by Besse (2016). It is of importance to know the laboratory experimental setup, as the parametric optimization was done using the combined results from Besse (2016) and the current study.

3.3 Field Site Investigations

From May 2016, field site investigations were done for testing the device's functionality. The devices were initially constructed by Pierce Industries, LLC., and were transported to the study location with the help of the University of Louisiana at Lafayette research team. The team helped the installation of the units, building the walking bridges and setting up the control site for data measurement purposes.

3.3.1 WSSC Units

The units tested for the field study were full-scale models of the technology. They were constructed by Pierce Industries, LLC., and the dimensions were 1.52 m x 1.37 m

(height x width) with 0.15 m diameter pipe openings. Figure 9 below shows the depiction of the field units.

Figure 9: WSSC Units after Construction

3.3.2 Location of Study Site

After carefully evaluating four sites, the Cut Off, LA levee site was chosen for the field investigations because of its transportation access, feasibility of data collection and availability of resources. The location of the field site is shown in Figure 10 where the marker indicates the town of Cut Off in Louisiana and the red arrow indicates the specific location of the site in the levee district. Researchers surveyed the study site carefully for construction feasibility in May 2016 (Figure 11). After the initial survey a suitable spot was marked where the units could be transported easily and could be put into the water using the crane without disturbing the natural balance in the shoreline.

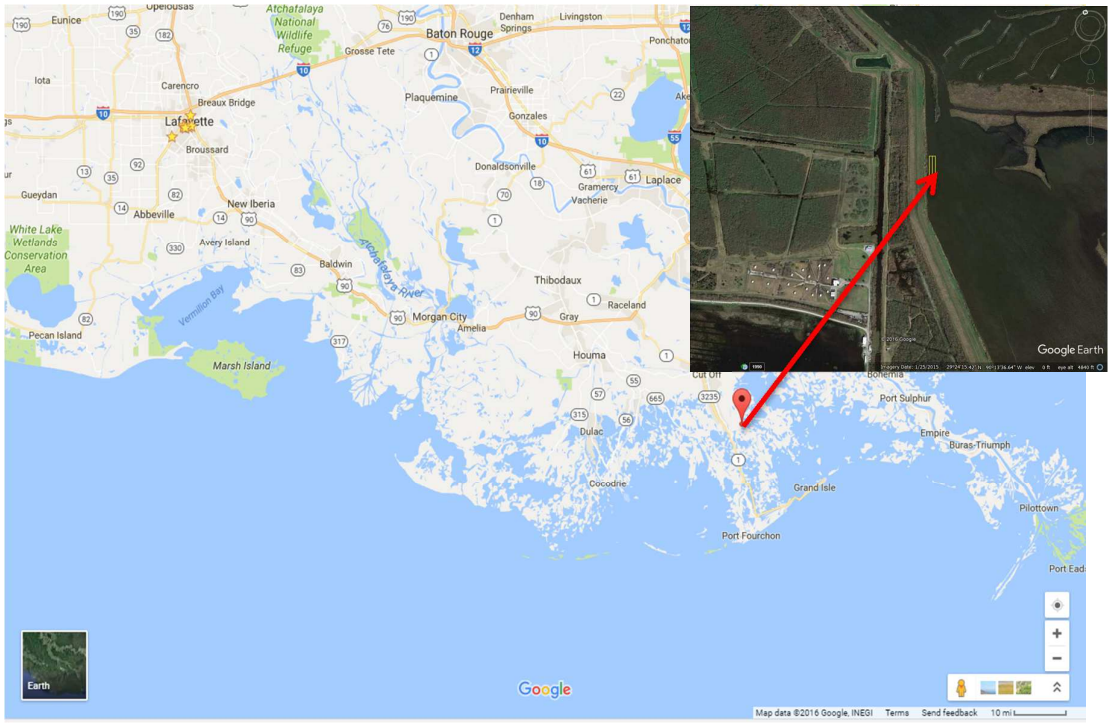

Figure 10: Location of the Field Site in Cut Off, LA

Figure 11: Initial Survey at the Field Site (May 2016)

3.3.3 Field Installation of WSSC Units

The units were transported to the site on the back of a moving truck and put in place by the research team. A Caterpillar crane was used for the ease of lifting the units from the shoreline and putting them in water. The research group then floated the units and moved them to the desired location. The units were then filled with water so that they sank down to the bed. Units were filled in such a way that no stress is created on the soil bed and the units sit gently on the surface. The main purpose of this is to prevent damage to the subsurface soil near the coast, which would create more loose soil for erosion. Figures 12 and 13 illustrate the process of installation of the units.

Figure 12: WSSC Units Being Installed in the Site

Figure 13: WSSC Units Being Filled with Water and Placed at Site

After the units were put in place and bound together, they were anchored using steel rod anchors to eliminate the lateral movement of the units due to the wave action.

Figure 14: WSSC Units after Construction

A wooden bridge was constructed in the study site so that future surface elevation measurements could be taken easily without disturbing the soil surface and equilibrium behind the units. Figure 14 and 15 show the final layout of the units after construction and the study site with the wooden bridge, respectively.

Figure 15: WSSC Units with Wooden Bridge for Walking

3.3.4 SET Survey

After the installation of the WSSC units, the plot behind the units was divided into grids for taking monthly elevation change measurements. Figure 16 shows the layout of the field site with the surveying points of the SET and plot locations of the marker clay experiment. The plot had a total of six columns and five rows, sequentially labeled from A-F and 1-5 respectively. A reference point was selected at the shoreline which was used to specify the location of the Total Station (equipment used for surveying) and to standardize the elevation data from field site and control site. Figure 17 shows the surveying technique for taking SET measurements using a total station and measuring staff. The data from the surveying were plotted on a monthly graph to see the elevation change behind the units over time.

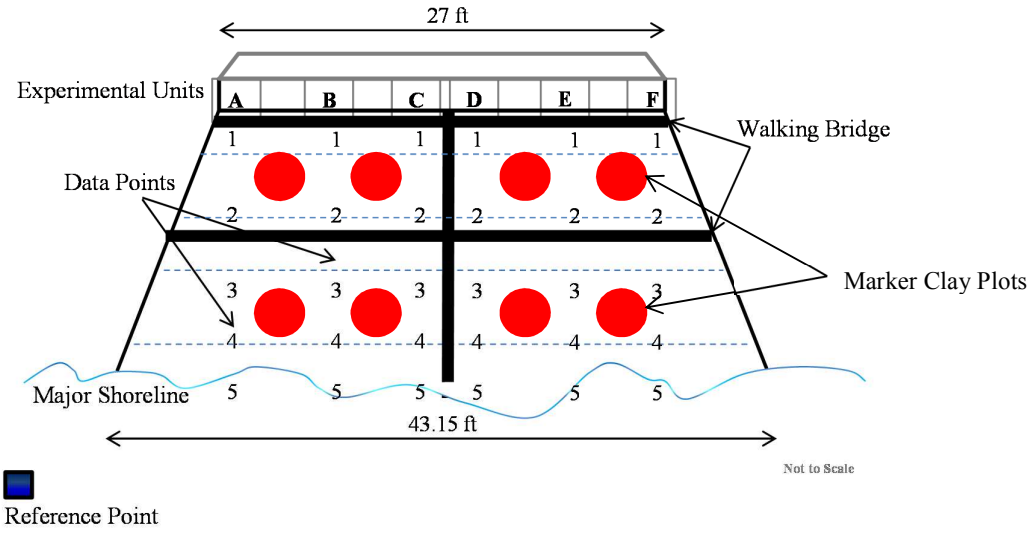

Figure 16: Layout of the SET Surveying and Marker Clay Experiment Site

Figure 17: Surveying Technique for SET Measurements

To compare the performance of the experiment site with the natural coastal environment, a control site was chosen close to the field site. Monthly data was taken at the control site to see the elevation change and erosion rate without any shoreline structures. Figure 18 illustrates the layout of the surveying points for the control site. The same measuring technique was followed as the experiment site but due to the absence of a walking bridge at the control site, the measurements were taken using a boat.

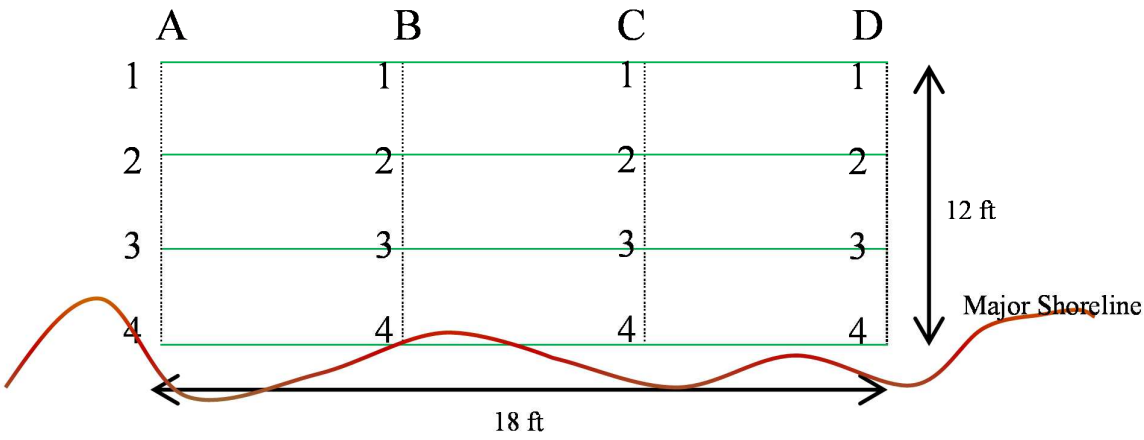

Figure 18: Layout of the SET Surveying at Control Site

3.3.5 Marker Clay Experiment

To confirm the data collected from the surface elevation tables, Feldspar clay was spread across all over the plot and eight distinct circular plots were marked with heavy Feldspar deposition in November 2016. Figure 16 and 19 shows the plot locations and how the circular marker clay plots were created in a submerged environment respectively.

Figure 19: White Feldspar Clay Being Deposited for Future Experiment

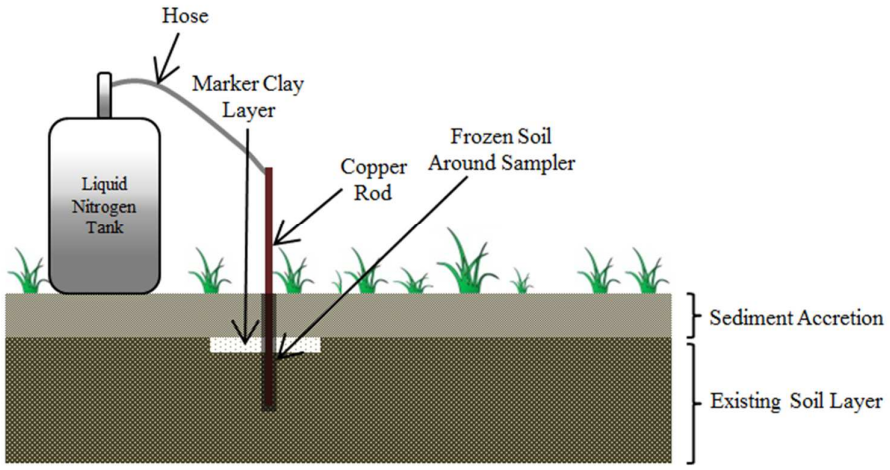

Figure 20: Standard Soil Coring Technique for Damp Soil in Wetlands

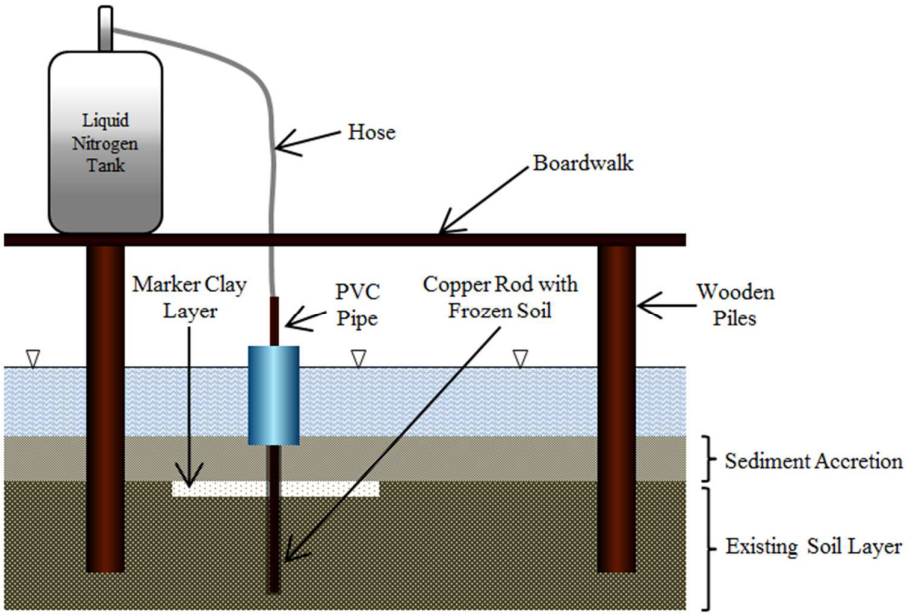

Figure 21: Modified Soil Coring Technique for Submerged Condition

Later on, soil coring was performed to check the sediment buildup over the Feldspar clay using liquid nitrogen and copper rods. Initially, the method to freeze soil cores in a submerged condition using liquid Nitrogen was difficult as standard operation procedure suggested a freezing time of 30-40 seconds. That process was derived to freeze soil cores in a damp soil condition in the wetlands which was not the case in the

experiment site. The study site had significant amount of water over the soil bed. Due to the submerged conditions, it was very difficult to freeze the soil as the water was impeding the freezing process around the copper rod. Thus, a modified technique was adopted to successfully perform the sampling. Figures 20 and 21 show the standard soil coring technique in a damp soil condition and the modified technique adopted in this study for a submerged coastal environment.

Firstly, a hollow PVC pipe with a diameter of 0.15 m was placed into the marker plots. Water was then pumped out from the inside of the pipe using a hand pump. When there was little amount of water inside the pipe, the copper sampler rod was driven into the plots and liquid nitrogen was allowed to flow through the hose into the copper rod. As the copper rod got colder, wet soil around it started to freeze and get attached on the body of the rod. Longer freezing time of 5-6 minutes was required to get solid soil cores and pictures were taken quickly before the core melted into mud again. Figure 22 illustrates how the actual coring was down using the modified technique.

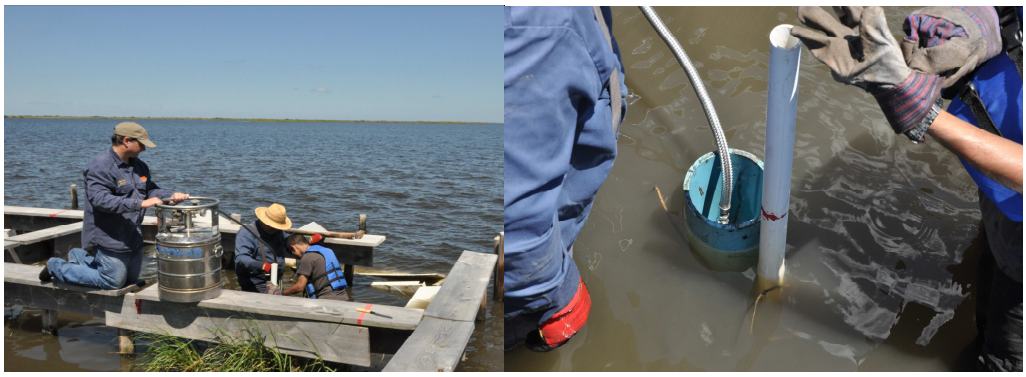

Figure 22: Soil Coring at the Study Site

CHAPTER 4: RESULTS AND DISCUSSION

4.1 Sediment Transport Modeling

The model was run for about 36 hours to get sediment transport data of over 60 seconds. The assigned monitors for different computational zones produced concentration graphs based on sediment availability in the water. The sediment concentration graphs were volume weighted average (kg/m^3) of defined silt particles. Figure 23 and 24 shows a sample monitor output from Ansys FLUENT indicating concentration curves from the front and back sides of the unit gradually decreasing and increasing over time.

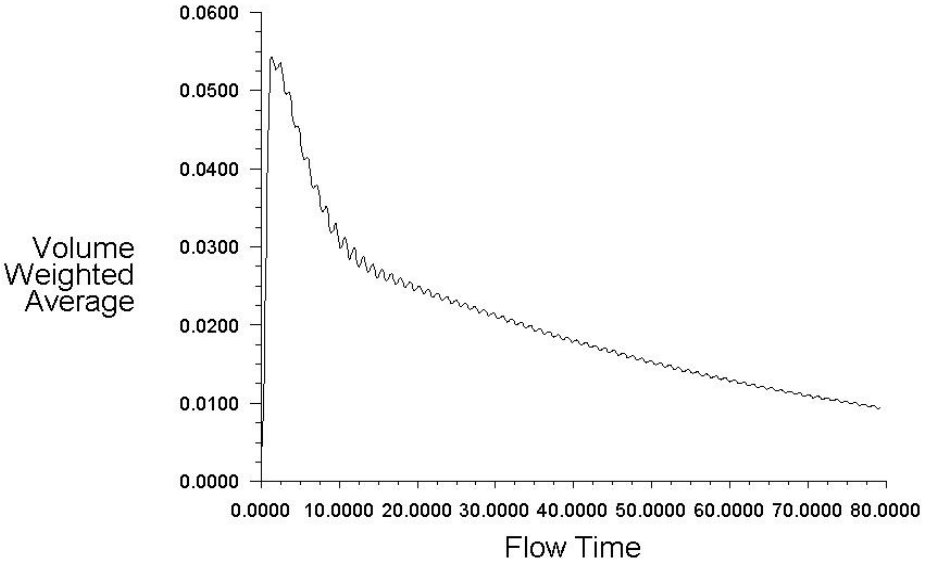

Figure 23: Sample FLUENT Monitor Output for Front Zone of the Tank

The concentration data both in the front and back of the units was also exported as comma separated values (.csv) files, and then the data were linearized and converted into Mass vs. Time plots in MS Excel.

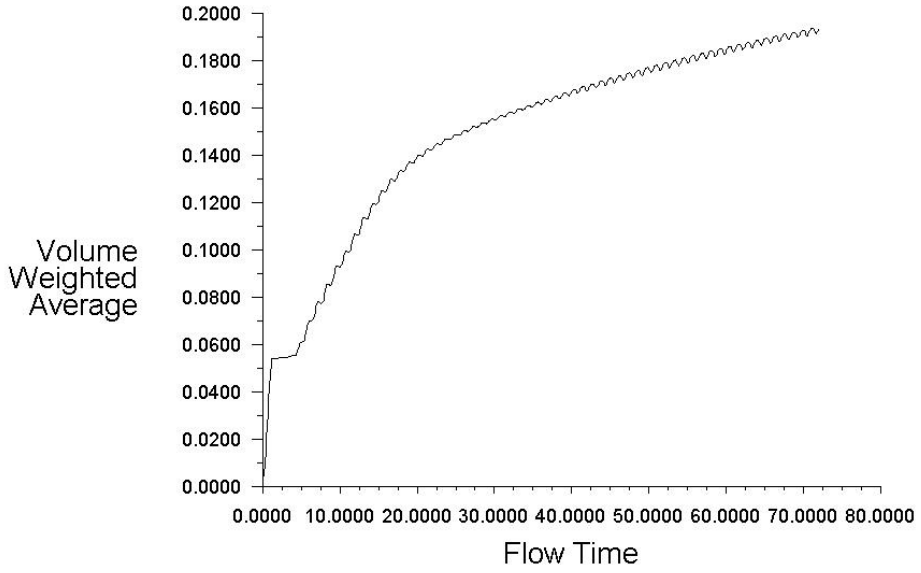

Figure 24: Sample FLUENT Monitor Output for Back Zone of the Tank

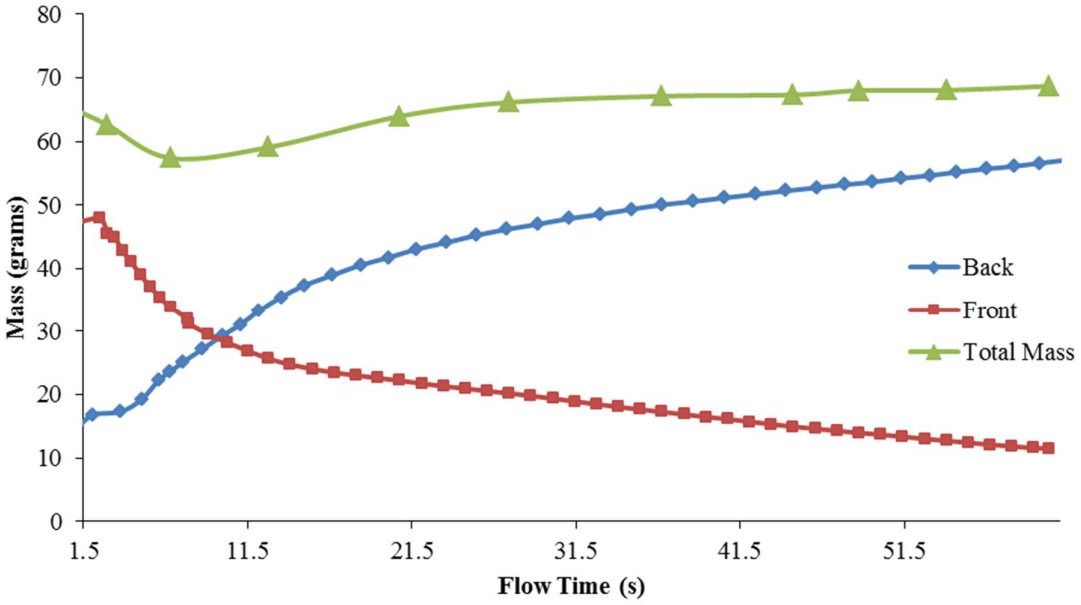

Figure 25: Sample Mass vs. Time Plot for Sediment Transport Simulation

A sample Mass vs. Time plot includes the mass balance curve i.e., total mass inside the tank over time (Figure 25). The total mass line is not perfectly flat because in this computation the middle zone containing the unit was considered negligible.

4.1.1 Pipe Diameter Effect

Different unit geometries were simulated in FLUENT to understand the effect of pipe diameters on the sediment transport efficiency. The mass transport results show that at the end of the first 20 seconds, significant differences in sediment transport were observed for units with different diameters, with the design of smaller diameters having less sediment transport (Figure 19). However, the difference diminished as time went on. At the end of the first 60 seconds, the simulation results showed marginal differences in sediment transport between designs of different pipe diameters.

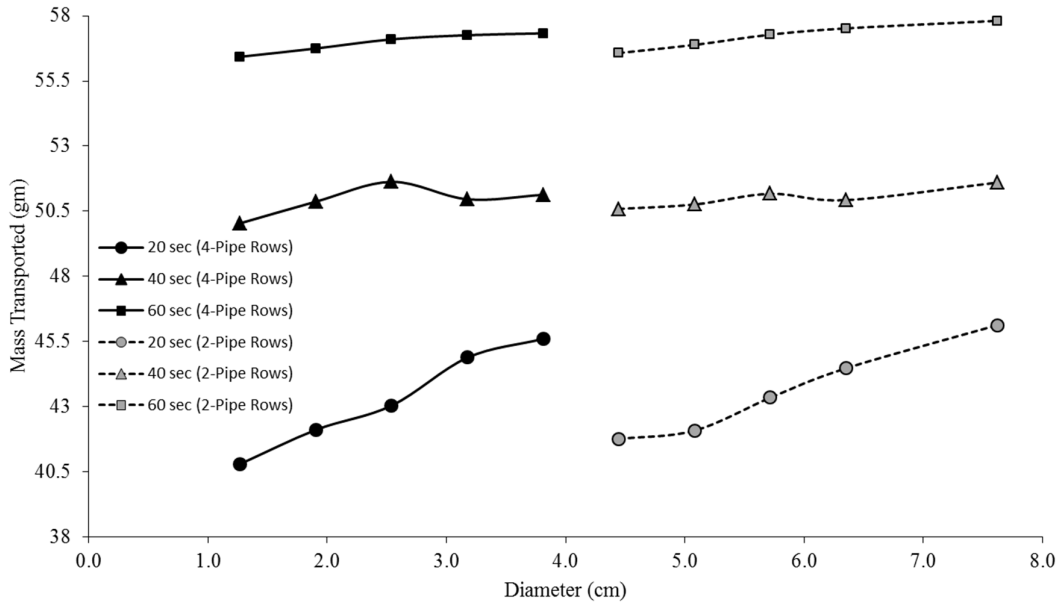

Figure 26: Time Comparison of Sediment Transport for Different Diameters

Figure 27 shows the total sediment transport results from two designs of 4-pipe row and 2-pipe row geometries at the end of the first 60 seconds. Figure 27 shows that the design of the smaller pipe diameter tends to have less sediment transport regardless of variations in the number of pipe row. Smaller pipe diameters directly lead to less sediment that can travel to the back of the unit in a single wave. Also, suspended sediments tend to settle down with time, which reduces the available particles in the water

column. In addition, smaller pipe diameters cause more wave reflection and turbulence that might also affect the mass transport.

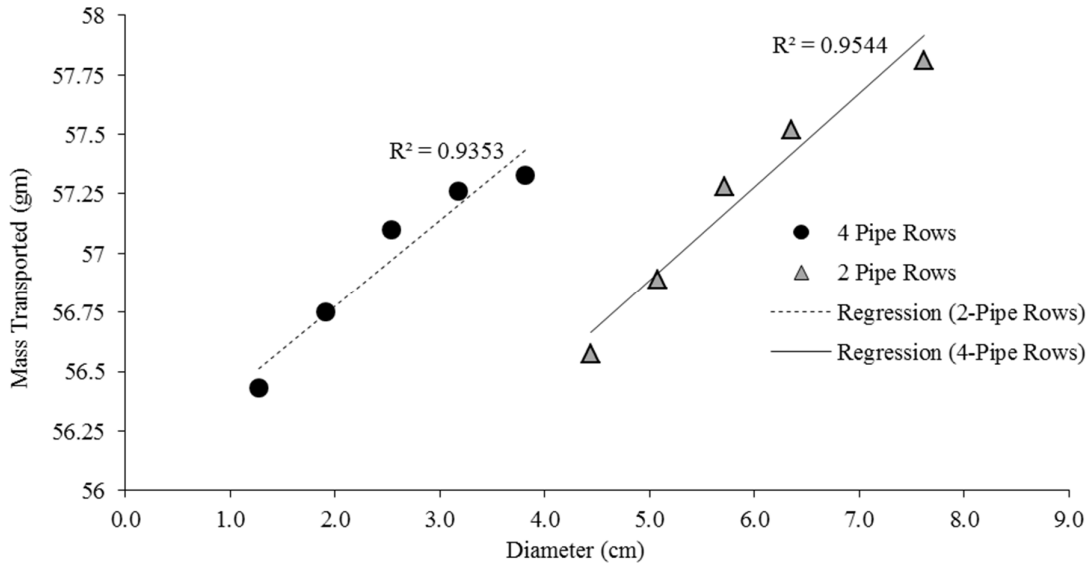

Figure 27: Mass Transport in 60 seconds (2 and 4-Pipe Row Units)

Linear regression and statistical analysis were conducted on the simulation results shown in Figure 27. It was found that the results were statistically significant for both 4-pipe row and 2-pipe row geometries. The R-square and p-values for the 4-pipe row geometries were 0.94 and 0.007, whereas they were 0.97 and 0.014 respectively for the 2-pipe row geometries. Both statistical analyses indicated that the trend is significant, and the parameters, namely mass transport and pipe diameter, are correlated statistically. Thus, it can be concluded that larger pipe diameters in the geometries yield higher sediment transport.

4.1.2 Face Slope Effect

Figure 28 shows different face slope effects on sediment transport. The sediment transport was negatively affected as the ratio (H/L) increased from 0.4 to 0.8.; at the ratio of 0.8, a minimum value was observed. At H:L= 1.0, the unit reaches maximum efficiency and again starts decreasing from the peak. Figure 28 also represents the mass

transport with the changing of face slope (H/L) for a relative depth (water level/wavelength) of 0.13. A statistical analysis was run on the results obtained for the slope study, and it was found that the results were statistically insignificant to draw any conclusions for sediment transport efficiency. Machado et. al. (2012) found similar results for mass transport; however, their design had the peak mass transport at H/L = 0.4.

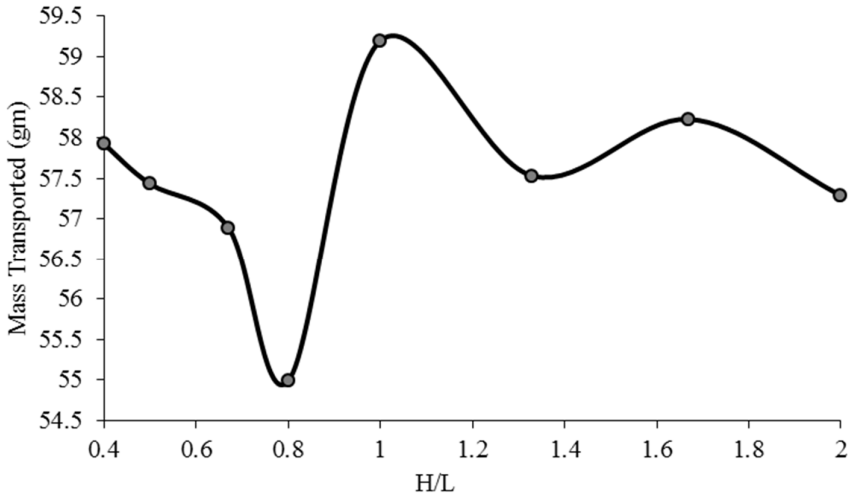

Figure 28: Mass Transport vs Face Slope (H/L)

4.1.3 Parametric Optimization of WSSC

To better serve the goal of the study, the wave reduction data from the previous study (Besse, 2016) and sediment transport simulation results from the current study were both plotted against the geometric porosity of the units. The wave reduction data in Figure 29 shows a declining trend with increasing porosity (open to total area, A_o/A_T), i.e., the higher the percentage of open area on the WSSC, the lower wave reduction can be achieved. Mass transport and porosity data were plotted in Figure 30, and the trend revealed that increasing porosity results in higher sediment transport. Increasing porosity can be attributed to larger pipe diameters and openings. Both the figures strengthen the conclusion of the diameter study results (Besse, 2016). Also, the wave reduction and mass transport data were both found to be statistically correlated with geometric porosity.

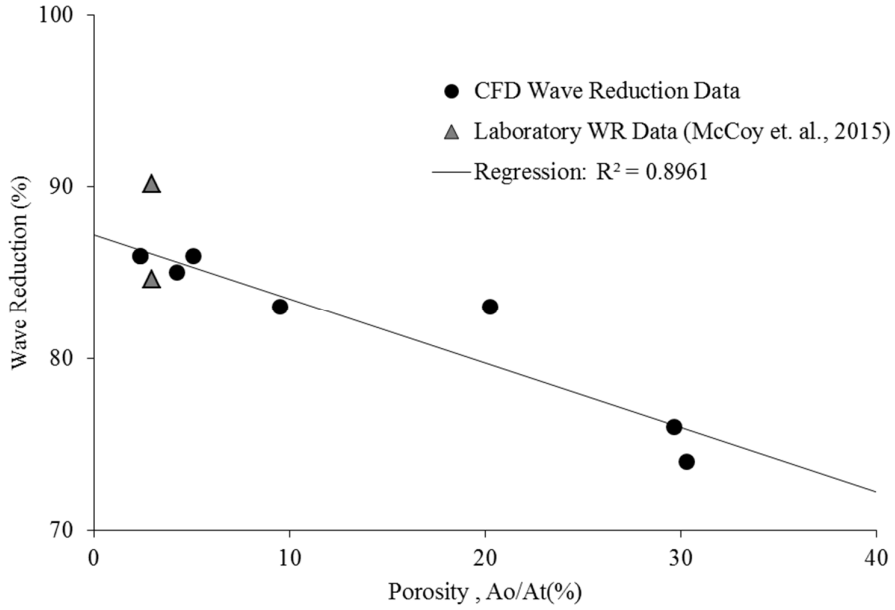

Figure 29: Wave Reduction vs Porosity Graph

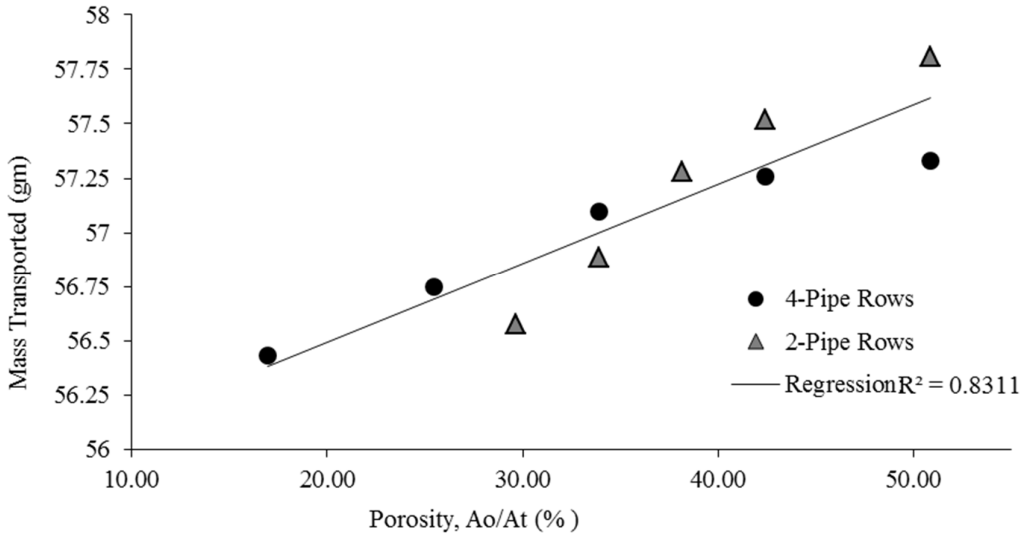

Figure 30: Mass Transport vs. Porosity Graph

In Figure 29 it can be observed that the laboratory measurements and CFD simulations at 3% porosity resulted in wave reduction in the range of 80-90%. However, even at the porosity of 30%, resultant wave reduction was around 75%. Though the porosity increased 10 times, the wave reduction did not decrease significantly. From

Figure 30, it can be seen that the mass transport was satisfactory at around 30%. As there has to be a balance of wave reduction and sediment transport in the optimized design of the WSSC, 30% porosity is recommended, which should provide satisfactory wave reduction and sediment transport.

4.2 Field Site Investigations

4.2.1 SET Measurements

Monthly data for the surface elevation table (SET) surveying was collected and plotted into a time-comparison graph. Figures 31-36 show the results of the SET measurements for grid line A-F. Figures 37-41 explain the sediment accretion on the horizontal lines 1-5 (rows) of the grid behind the units. In these graphs, point 1 indicates that it is close to the back of the units and point 5 indicates that it is close to the shoreline. The initial surveying was done immediately after the installation of the WSSC units in the field site, and was only done for the first 4 points. Later, one more point was added in the shoreline in the surveys for a more comprehensive picture about the sediment accretion process. The elevations shown here are relative to the reference point in the shoreline.

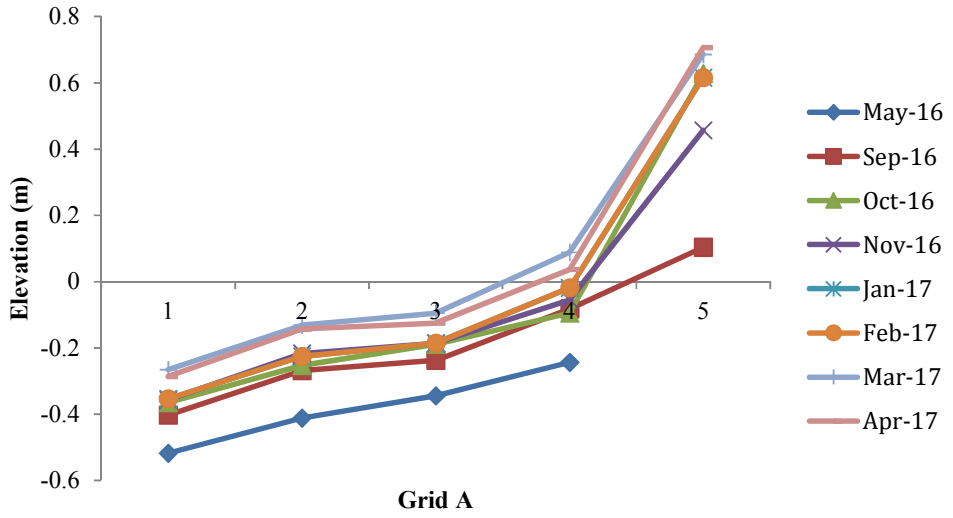

Figure 31: SET Measurements for Grid A

Figure 31 shows the elevation change in the grid line A from May 2016 to April 2017. Grid line A is the leftmost line in the experimental site. The sediment accretion (elevation change) on points 1-3 over the surveying period of 11 months were 0.25 m, 0.28 m, and 0.25 m. Usually it is seen that the elevation change is higher in the second point, as sediment particles do not settle quickly after entering the system. Because of the particle settling velocity of the silt particles, sediment travels a distance behind the units before settling in the region where point 2 is located. Accretion on the fourth point was higher at 0.33 m during the May 2016 - April 2017 period. The fifth point which is closest to the shoreline had an accretion of 0.58 m over the period of nine months (September 2016-April 2017). This high elevation change can be attributed to the gradual breaking of lands towards the sea. This might have also contributed to the higher than average accretion around point 4. It is also seen that sediment accretion occurred more in the summer and spring months due to high water level and sediment availability. Low accretion was observed in the winter months which can be attributed to the low water level in the sea during winter. Overall, a good amount of accretion was observed in this line which is on average (1-4 points) 0.28 m.

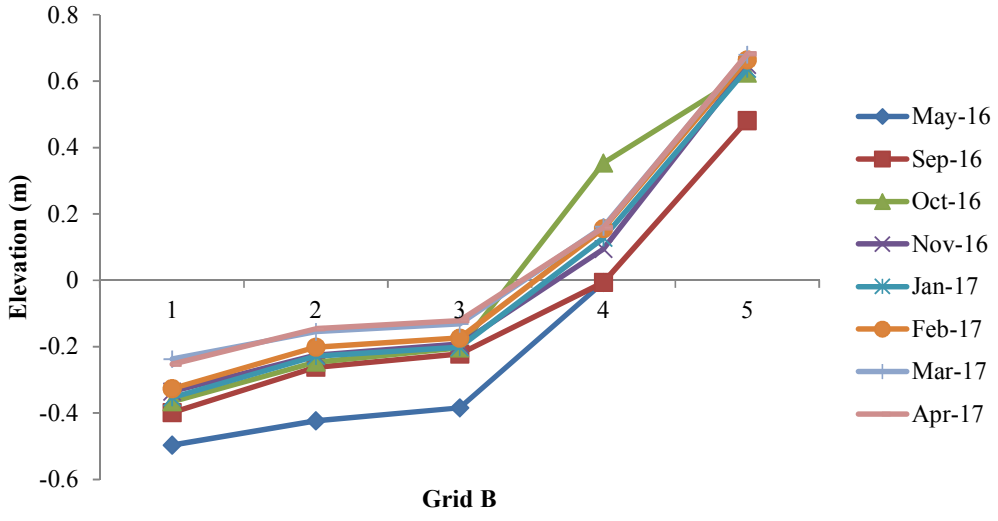

Figure 32: SET Measurements for Grid B

Figure 32 shows the elevation change in the grid line B from May 2016 to April 2017. The sediment accretion (elevation change) on points 1-4 over the surveying period of 11 months were 0.24 m, 0.28 m, 0.26 m, and 0.16 m. Like grid line A, grid line B also shows more accretion on point 2. The fifth point had an accretion of 0.20 m over the period of nine months (September 2016-April 2017). This shows that there was not much land breakage and soil dissipation into the water from the shoreline as both point 4 and 5 did not have high elevation changes. On an average (points 1-4), 0.23 m of accretion was observed. Another observation is, sediment accretion occurred more in the regions closer to the units and the amount decreased towards the shoreline.

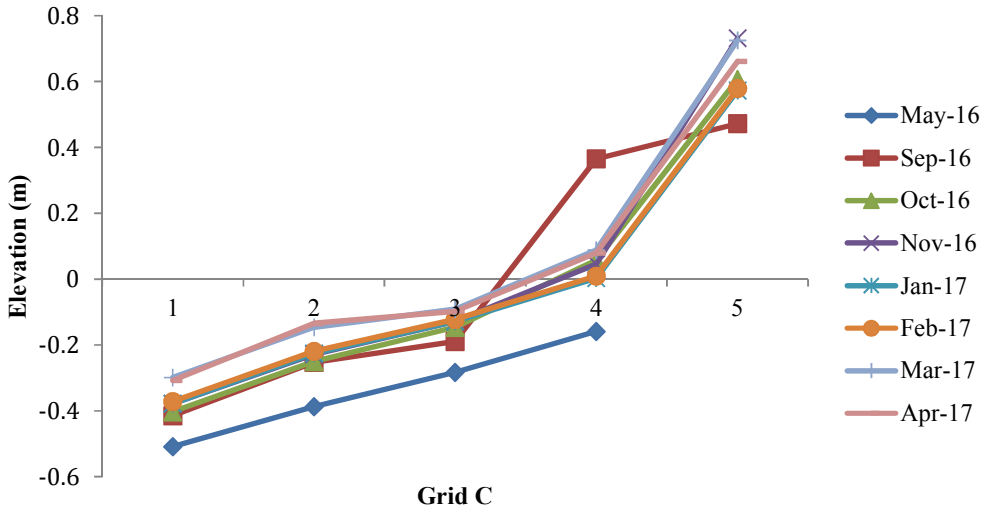

Figure 33: SET Measurements for Grid C

Figure 33 shows the elevation change in the grid line C from May 2016 to April 2017. The sediment accretion (elevation change) on points 1-4 over the surveying period of 11 months were 0.20 m, 0.25 m, 0.19 m, and 0.24 m. Similar to previous lines, grid line C also shows more accretion on point 2. The fifth point had an accretion of 0.19 m over the period of nine months (September 2016-April 2017). Similar to the previous point, this shows that there was not much land breakage and soil dissipation into the

water from the shoreline as both point 4 and 5 did not have very high elevation changes. On an average (points 1-4), 0.22 m of accretion was observed. Also, surveying line from September 2016 has an unusual peak at point 4 which might have been caused by human error while taking the measurements.

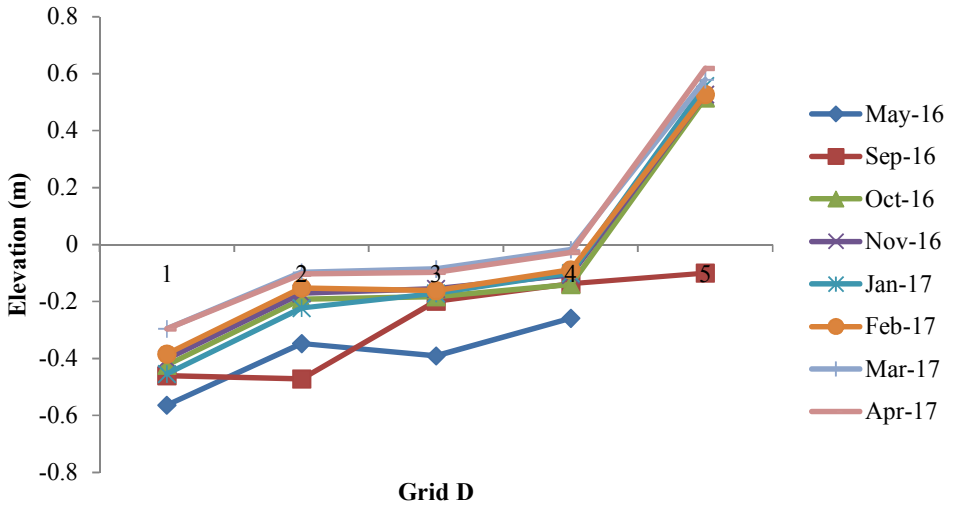

Figure 34: SET Measurements for Grid D

Figure 34 shows the elevation change in the grid line D from May 2016 to April 2017. The sediment accretion (elevation change) on points 1-4 over the surveying period of 11 months were 0.27 m, 0.24 m, 0.28 m, and 0.23 m. Unlike previous lines, grid line D shows more accretion on point 3. This might be the result of more sediment particles coming from both sides of the units and settling further in the middle where turbulence is the minimum. The fifth point had an accretion of 0.72 m over the period of nine months (September 2016-April 2017). The initial surveying of point 5 in September 2016 is unusually low compared to elevation measurements from other months. It might have been caused by a sudden landform change after the September 2016 survey. On an average (points 1-4), 0.26 m of accretion was observed.

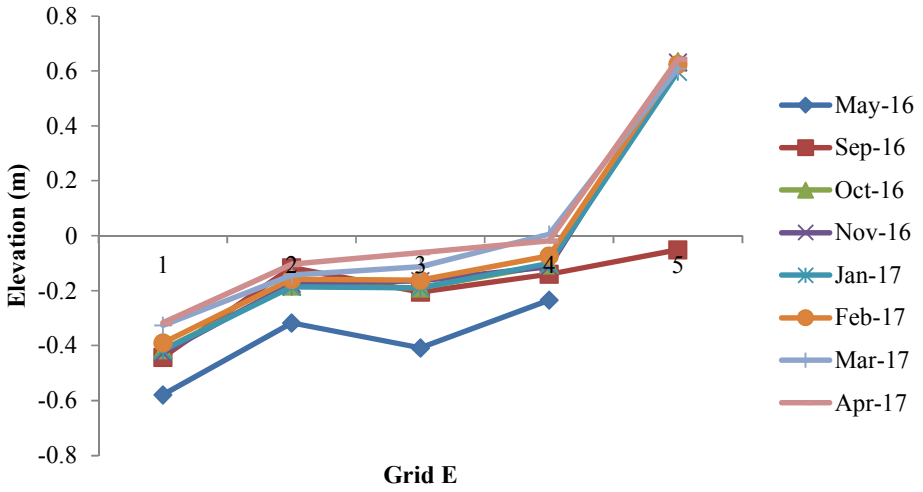

Figure 35: SET Measurements for Grid E

Figure 35 shows the elevation change in the grid line E from May 2016 to April 2017. The sediment accretion (elevation change) on points 1-4 over the surveying period of 11 months were 0.26 m, 0.21 m, 0.35 m, and 0.22 m. Similar to the previous lines, grid line C shows more accretion on point 3. The fifth point had an accretion of 0.69 m over the period of nine months (September 2016-April 2017). Like point C, the initial surveying of point 5 in September 2017 is very low compared to elevation measurements from other months that can be attributed to the result of sudden landform changes in the shoreline due to land breakage. An average (points 1-4) of 0.26 m of sediment accretion was observed. Sediment accretion occurred un-uniformly behind the units which might be attributed to the right side location of this grid line E that faces more turbulence due to wind direction.

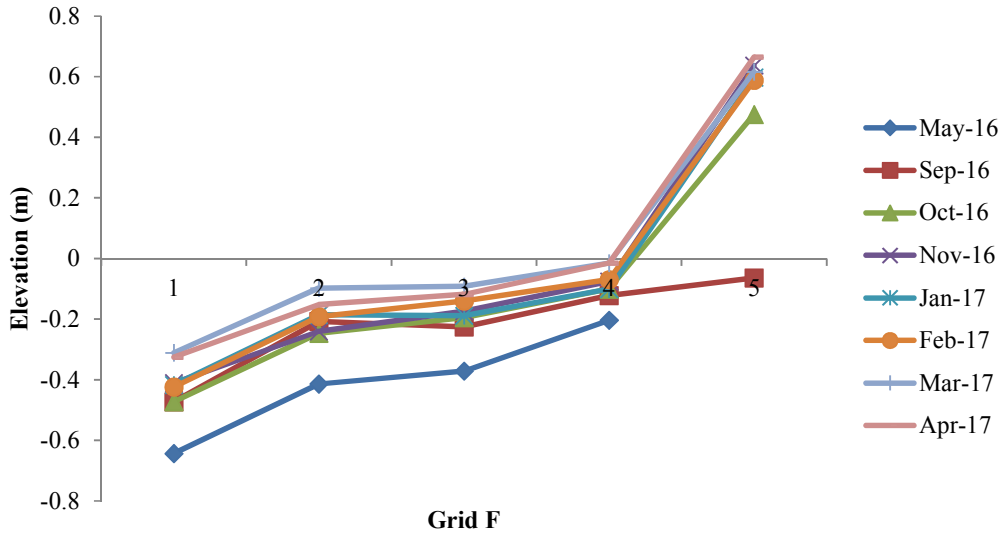

Figure 36: SET Measurements for Grid F

Figure 36 shows the elevation change in the grid line F from May 2016 to April 2017. The sediment accretion (elevation change) on points 1-4 over the surveying period of 11 months were 0.32 m, 0.26 m, 0.25 m, and 0.18 m. Unlike all previous lines, the first point on grid line F had the highest accretion which can be attributed to the water waves' angle of hitting the units. Larger particles immediately settled down near point 1 after losing momentum because of the WSSC units. Sediment accretion gradually decreased from points 1-4 in this line which might also be the result of wave angle. The fifth point on this line had an accretion of 0.73 m over the period of nine months (September 2016-April 2017). Like the points on line D and E, the initial elevation of point 5 in September 2017 is very low compared to elevation measurements from other months. The sudden change might have caused by landform change due to landslide. On an average (points 1-4), 0.26 m of accretion was observed.

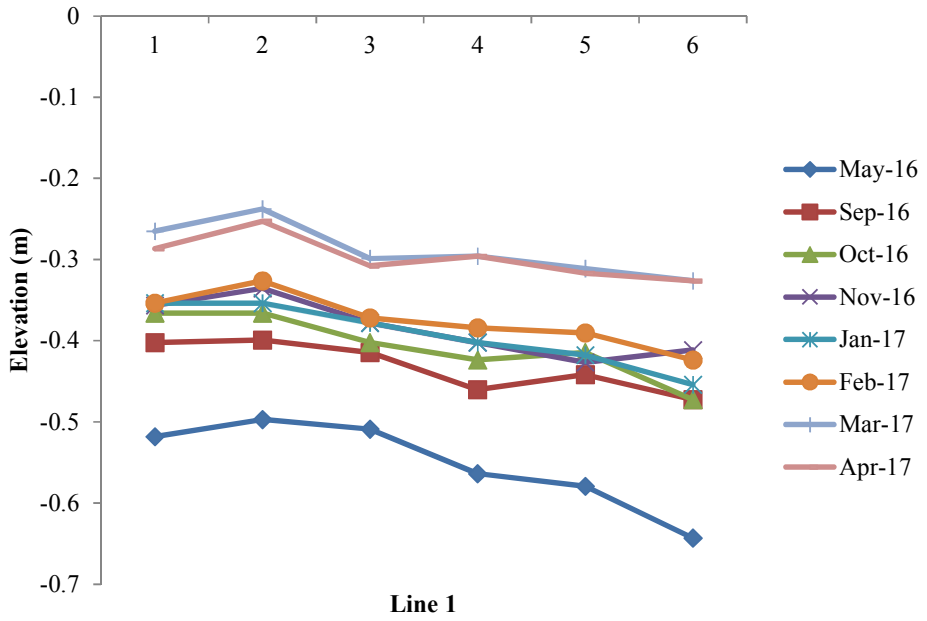

Figure 37: SET Measurement for Horizontal Line 1

Figure 37 shows the elevation change in the horizontal line 1 from May 2016 to April 2017. It can be clearly seen that higher accretion was observed in the summer and spring months when the water level was higher in the rivers and seas. Higher water level carries more sediment particles, and the WSSC units were able to retain more sediment behind them by reducing the velocity of water. On an average, 0.26 m of accretion was observed in the horizontal line 1. The right-side points retained more sediments as water was seen flowing angularly from the right-side due to wind direction. A stable and almost flat landform can be seen which proves the effectiveness of the WSSC in stopping erosion.

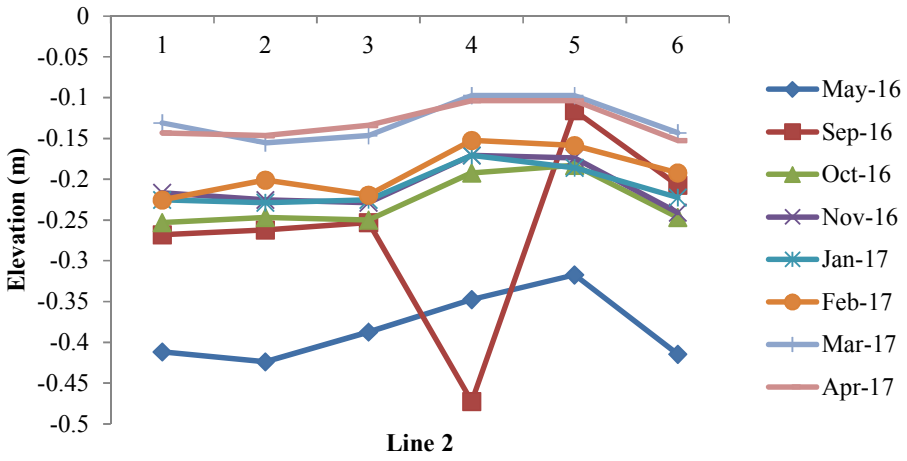

Figure 38: SET Measurement for Horizontal Line 2

Figure 38 shows the elevation change in the horizontal line 2 from May 2016 to April 2017. An unusually low and high elevation can be seen at points 4 and 5 respectively on the surveying line from September 2017. This might be the result of wrong placement of the surveying rod into a ditch or rock. Similar to horizontal line 1, an average of 0.26 m of accretion was observed along the horizontal line 2.

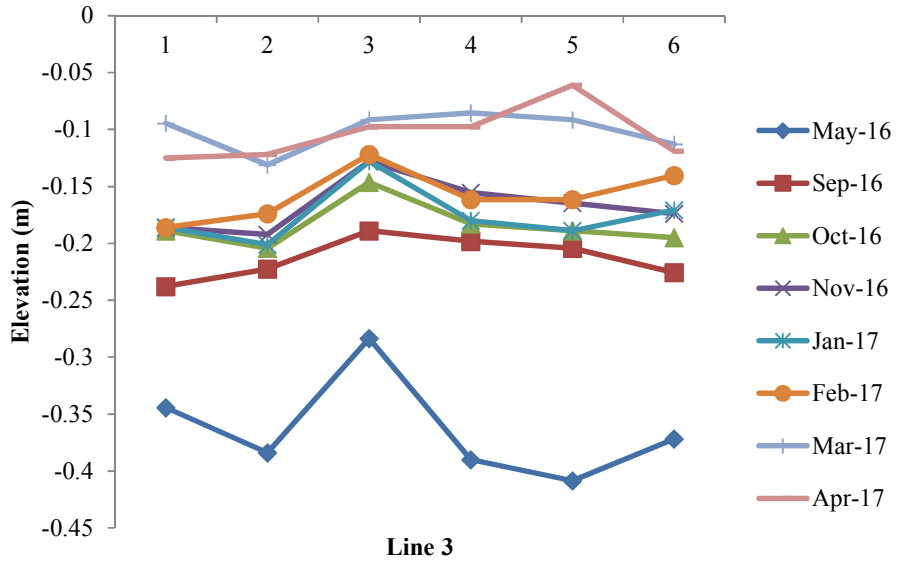

Figure 39: SET Measurement for Horizontal Line 3

Figure 39 shows the elevation change in the horizontal line 3 from May 2016 to April 2017. On an average, 0.26 m of accretion was observed in the horizontal line 3. The right-side points retained more sediments as water was seen coming angularly from the right-side due to wind direction.

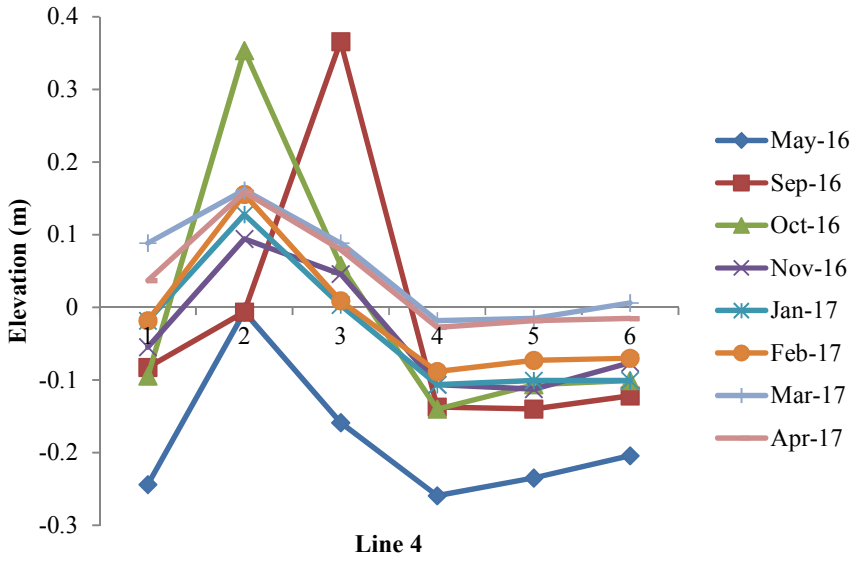

Figure 40: SET Measurement for Horizontal Line 4

Figure 40 shows the elevation change in the horizontal line 4 from May 2016 to April 2017. There were points where the sediment accretion was seen much higher than the previous points which might have been caused by sudden deposition of sediment at the place or human error during surveying. As the land slowly flattens down over time due to low turbulence, the peak points were later seen to have flattened. On an average 0.23 m of sediment accretion was observed along this line.

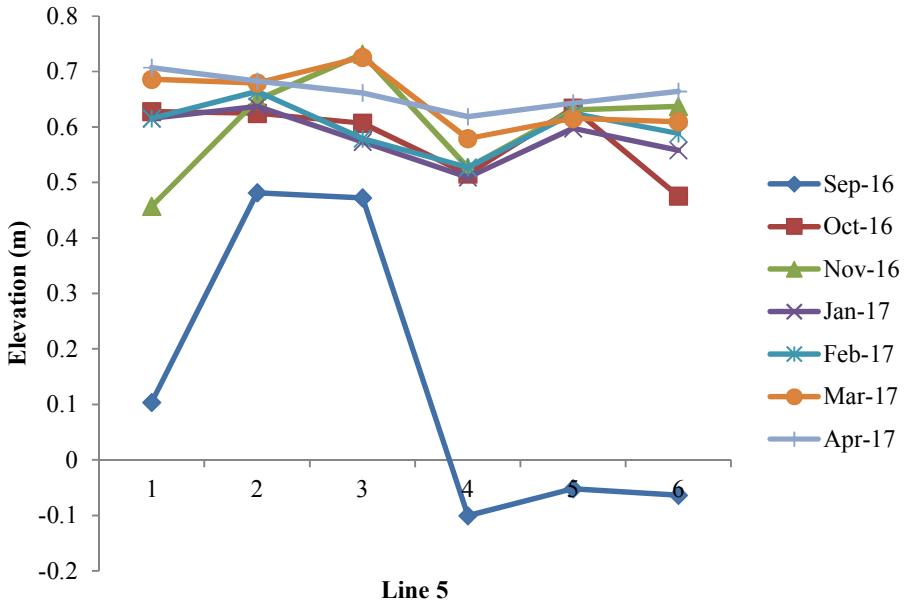

Figure 41: SET Measurement for Horizontal Line 5

Figure 41 shows the elevation change in the horizontal line 5 from May 2016 to April 2017. It is mentionable that line 5 represents the line closest to the shoreline. No erosion of the shoreline was observed in line 5 rather a good amount of accretion occurred in the time period. An initial survey showed low elevations in the shoreline right after installation was finished but after few months the shoreline reached equilibrium. From that point on, gradual sediment deposition occurred due to the performance of the WSSC units.

The SET surveys at the experiment site showed the effectiveness of the WSSC technology in stopping coastal erosion and helping land buildups behind the units. In most cases the average land buildup ranged from 0.21-0.27 m, which is a considerable amount over almost a year.

4.2.2 Control Site Measurements

Figure 18 shows the layout of the control site with the surveying points. Figures 42-45 represent the elevation change at the control site along the vertical grid lines A-D. Figures 46-48 show the elevation change along the horizontal grid lines 1-3.

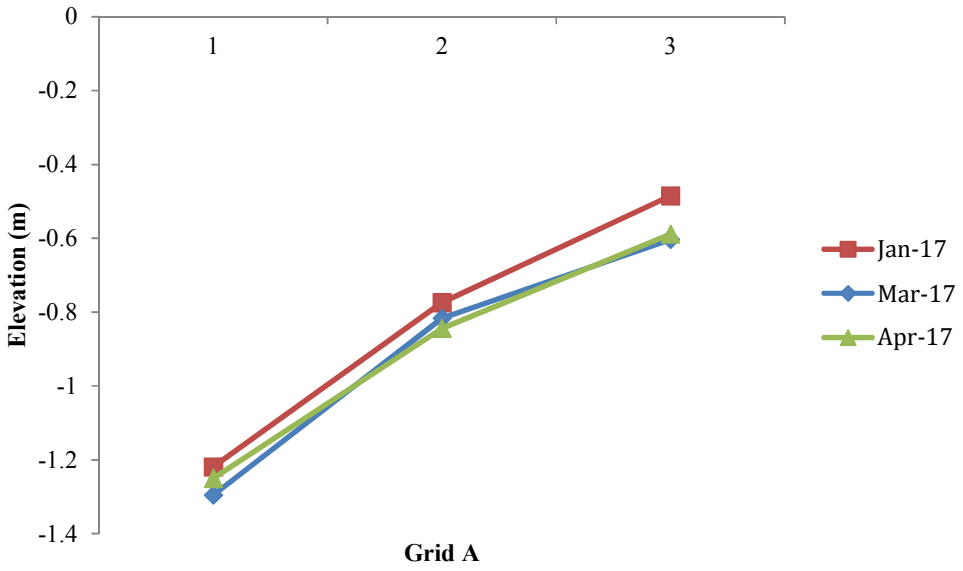

Figure 42: SET Measurement for Grid A (Control Site)

Figure 42 shows the elevation change through grid line A from January 2017 to April 2017 at the control site under natural erosion effects. Though the data is not sufficient to make decisive conclusions, a small amount of elevation decrease is observed all through the grid line. The point 1 refers to the point farthest from the shoreline into the water whereas point 3 is the closest from the shoreline. Like any general coastal land slope, the points 1 to 3 represent the sloped soil bed at the control site.

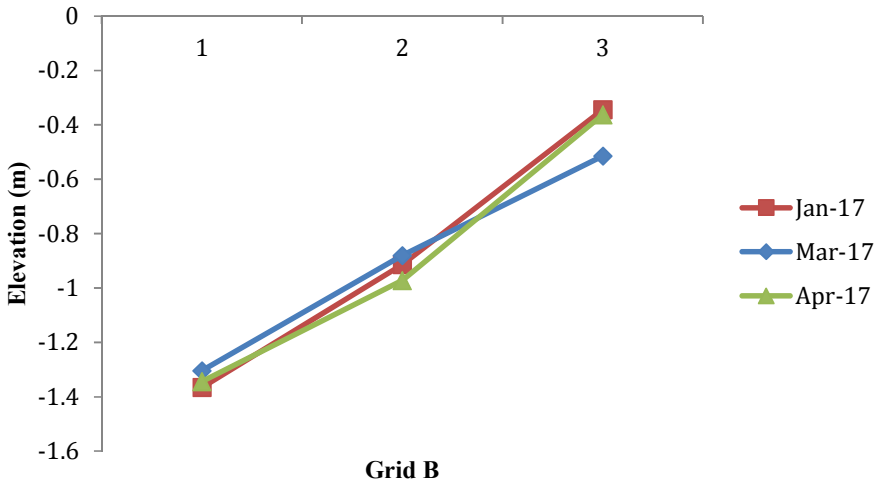

Figure 43: SET Measurement for Grid B (Control Site)

Figure 43 shows the elevation change through grid line B from January 2017 to April 2017 at the control site under natural erosion effects. The data is not sufficient to make any decisive conclusions as the three monthly lines overlapped and did not show much change in elevations.

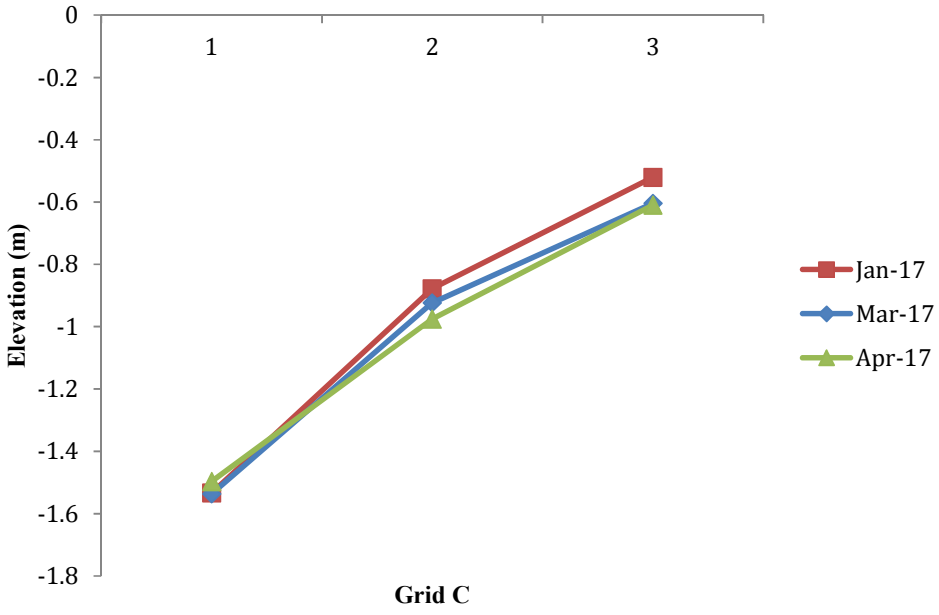

Figure 44: SET Measurement for Grid C (Control Site)

Figure 44 and 45 show the elevation change through grid line C and D respectively from January 2017 to April 2017 at the control site under natural erosion effects. A little loss of soil was observed at the shoreline point 3 on Figure 44. The data is not sufficient to make any decisive conclusions as no significant change in elevation was observed from the graph in both figures.

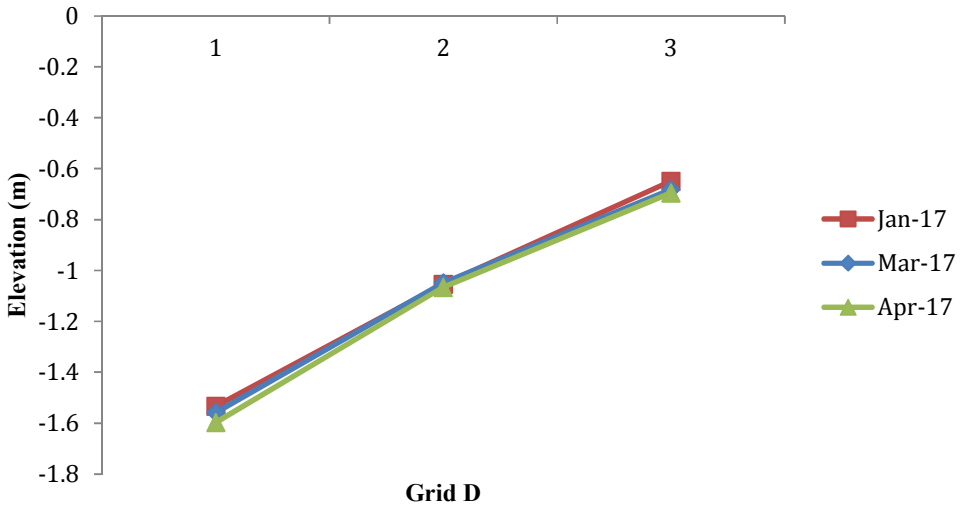

Figure 45: SET Measurement for Grid D (Control Site)

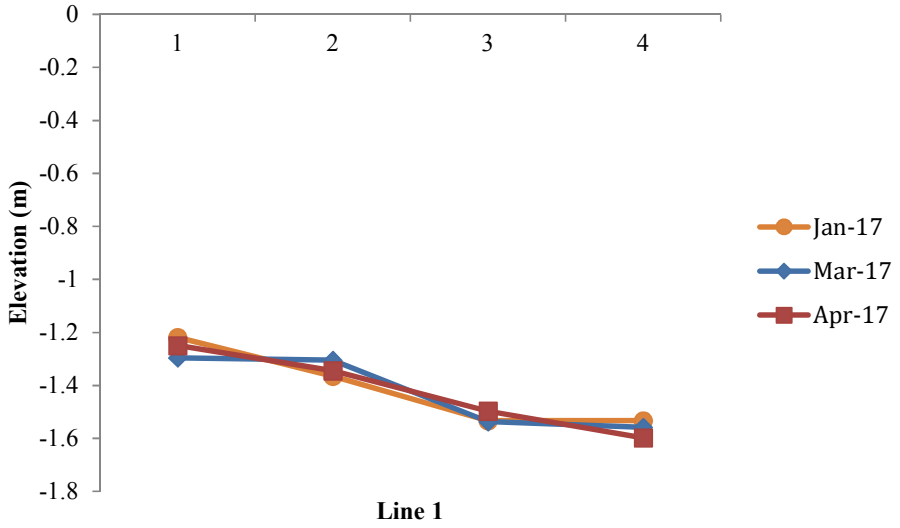

Figure 46: SET Measurement for Horizontal Line 1 (Control Site)

Figure 46 shows the elevation change through horizontal line 1 from January 2017 to April 2017 at the control site under natural erosion effects. The point 1 refers to the rightmost point whereas point 4 is the leftmost point on the line. The three monthly lines overlapped and did not show much change in elevations. The elevations were found to be lower on the right-hand site of the control site which might be caused by the wind and wave direction coming from the right side towards the shoreline.

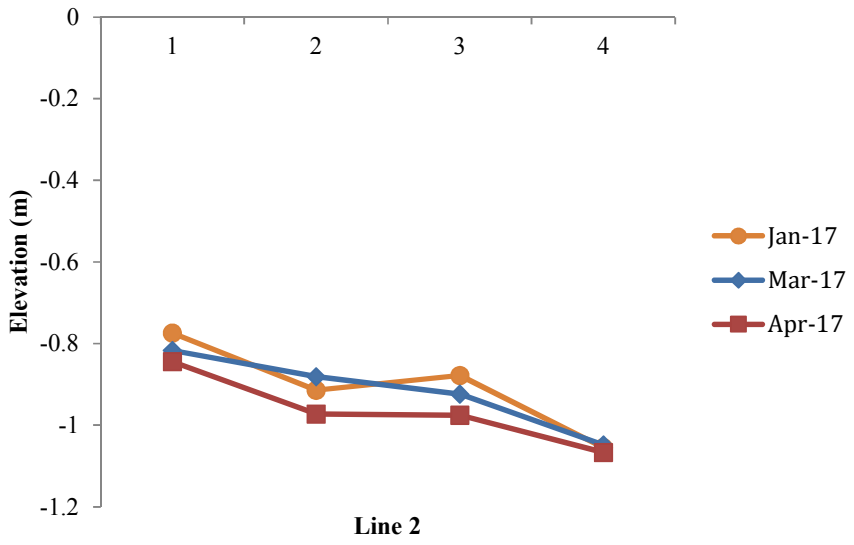

Figure 47: SET Measurement for Horizontal Line 2 (Control Site)

Figure 47 shows the elevation change through horizontal line 2 from January 2017 to April 2017 at the control site. Like the previous graph, the three monthly lines overlapped and did not show much change in elevations here.

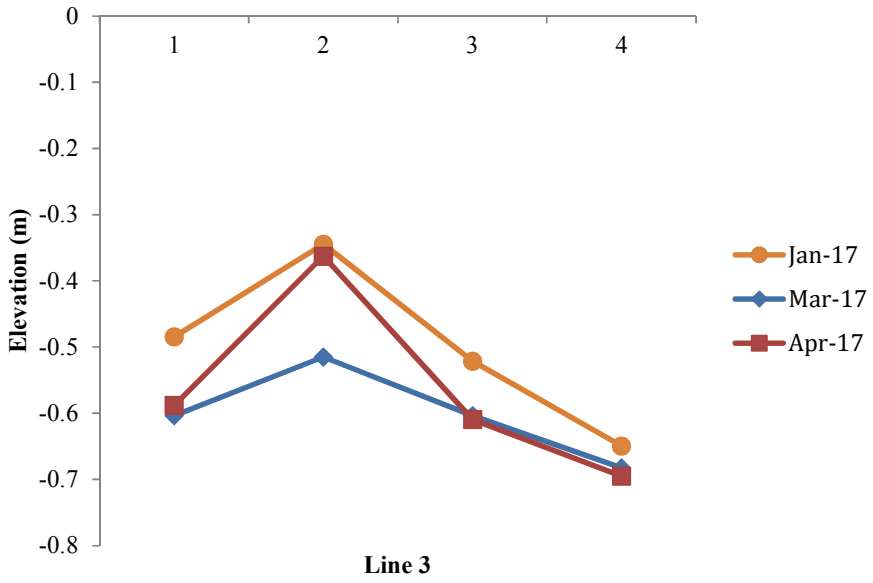

Figure 48: SET Measurement for Horizontal Line 3 (Control Site)

Figure 48 shows the elevation change through horizontal line 3 from January 2017 to April 2017 at the control site under natural erosion effects. The March elevation on point 2 was found lower than the April elevation. This might have been caused by wrongly placing the surveying rod into a ditch. It is mentionable that line 3 is the line that is closest to the shoreline. The significant change in elevation along this line might be attributed to the shoreline erosion due to unobstructed wave actions from the sea that results in gradual small landslides.

From the control site measurements, it was not possible to draw definite conclusions about the rate of erosion under natural wave actions. However, small amounts of negative elevation changes were observed and no significant accretion or sediment buildup was observed.

4.2.3 Marker Clay Experiment

Marker clay experiment was performed at the field site to confirm the SET surveying results. Among the 8 plots created for marker clay experiments as shown in Figure 16, only 2 plots could be successfully tested where the sediment accretion was

seen clearly over the white marker clay layer. Figure 49 shows the layout of the study site with successful and unsuccessful sampled plots. The black plots represent the unsuccessful ones whereas the red plots A and B indicate the successfully sampled plots.

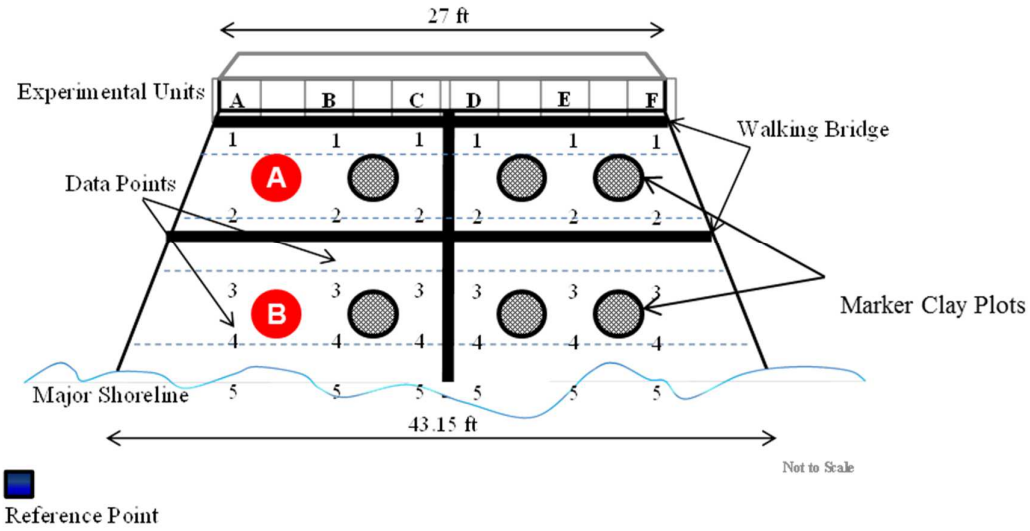

Figure 49: Layout of the Study Site with Successful and Unsuccessful Plots

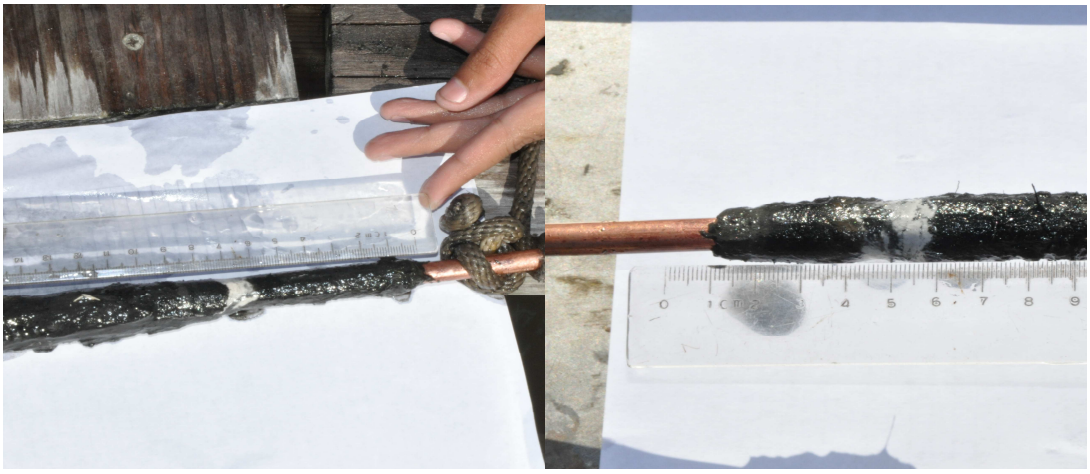

Figure 50: Sediment Buildup over Feldspar Clay (White) Layer

Figure 50 shows the soil core sample from plots A and B where a definite sediment accretion can be seen. Figure 51 shows the average of the SET measurements around plot A and B along with the accretion observed in those two plots. In the period of November, 2016 to April, 2017 the accretion from on points A-1, A-2, B-1, and B-2

points (Figure 49) were averaged and was found to be 0.0762 m for plot A. Similarly for plot B, the accretion of points A-3, A-4, B-3, and B-4 (Figure 49) were averaged and was found to be 0.0716 m. The marker clay accretions were 0.0699 and 0.06 m respectively for plot A and plot B.

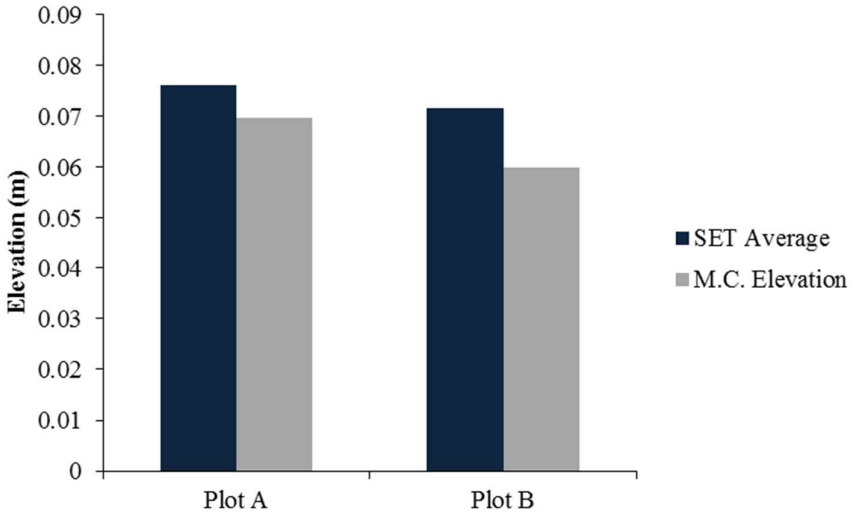

Figure 51: Comparison of SET and Marker Clay Accretion Results

The comparison shows that the SET measurements were consistent with the marker clay results. Both marker plots showed the sediment buildup in the range of 0.06-0.07 meters which was slightly lower than the average SET survey results. This might have been due to the loss of loose top soil during the pumping of water out at the place of the soil coring. Black slurry was observed while pumping out water which indicates loose sediment was also coming out with water. It is noticeable that when water was pumped out the volume of sediment in the column also decreased which might have resulted in difference with the SET survey results. Also, after freezing was done for the core, lot of twisting and shaking was needed to pull out the frozen core. This might have caused some soil at top of the rod and in contact with water to wash out.

CHAPTER 5: CONCLUSIONS

The main goal of this study was to model sediment transport data using currently developed CFD models, to optimize the design of the WSSC technology and to evaluate the performance of the technology in a field setting. CFD analysis showed consistent results compared with the results from physical modeling, indicating that the CFD models provided a reasonable representation of how the physical models behave. Results show that bigger diameters or pipe openings yielded higher mass transport. The results from the diameter study were statistically significant. However, there was no significant effect of face slope on sediment transport. The design of the WSSC was optimized using the simulated data from both the wave reduction and sediment transport study using porosity (open to total area ratio) as the common variable. It was found that optimum output for both wave reduction and sediment transport can be found at 30% porosity. However, this optimization may change slightly based on site-specific requirements. The field site investigations revealed that the WSSC units performed very well in an actual field setting. A modified technique was developed for marker clay sampling for a submerged environment using PVC pipes that involved pumping of water from inside the pipe to facilitate the freezing of cores. The Marker clay experiment confirmed the effectiveness of the WSSC technology in helping sediment accretion behind the units. Significant amount of sediment layer was observed over the white clay layer and the results were consistent with the SET surveying measurements. Thus, it can be concluded that the WSSC unit designs can be optimized using the results from the current study and can be used as shoreline protection structures to stop coastal erosion and land loss in Louisiana.

REFERENCES

Anderson, J. D., Wendt, J. 1995. Computational fluid dynamics, Springer.

Augustin, L. N., Irish, J. L., Lynett, P. 2009. Laboratory and numerical studies of wave damping by emergent and near-emergent wetland vegetation. Coastal Eng., 56, 332-340.

Besse, G., 2016. Analysis and Optimization of the Wave Suppression and Sediment Collection System: Sand Collection, Performance Characterization, and Computational Fluid Dynamic Modeling. M.S. Thesis, University of Louisiana at Lafayette, p. 69.

Birben, A. R., Özölçer, İ. H., Karasu, S., Kömürcü, M. İ. 2007. Investigation of the effects of offshore breakwater parameters on sediment accumulation. Ocean Eng., 34, 284-302.

Cavallaro, L., Dentale, F., Donnarumma, G., Foti, E., Musumeci, R. E., Carratelli, E. P. 2012. Rubble mound breakwater overtopping: estimation of the reliability of a 3D numerical simulation. Coastal Eng. Proc., 1, 8.

Coreil, P.D. 1995. Wetlands Functions and Values in Louisiana. Louisiana State University, Cooperative Extension Service and Sea Grant College Program, Baton Rouge, LA, and U.S. Environmental Protection Agency.

Costanza, R., Pérez-Maqueo, O., Martinez, M. L., Sutton, P., Anderson, S. J., Mulder, K. 2008. The value of coastal wetlands for hurricane protection. AMBIO: A Journal of the Human Environment, 37, 241-248.

Creel, L. 2003. Ripple effects: population and coastal regions, Population Reference Bureau, Washington, DC.

Day, J. W., Britsch, L. D., Hawes, S. R., Shaffer, G. P., Reed, D. J., Cahoon, D. 2000. Pattern and process of land loss in the Mississippi Delta: a spatial and temporal analysis of wetland habitat change. Estuaries, 23, 425-438.

Delaune, R. D., Patrick Jr, W. H., Smith, C. J. 1992. Marsh aggradation and sediment distribution along rapidly submerging Louisiana Gulf Coast. Env. Geol. and Water Sci., 20, 57-64.

Edwards, K. R., Proffitt, C. E. 2003. Comparison of wetland structural characteristics between created and natural salt marshes in southwest Louisiana, USA. Wetlands, 23, 344-356.

Fleming, C.A. 1990. Principles and Effectiveness of Groynes. Coastal Protection, Pilarczyk, K.W., (Ed.), Balkema Press, Rotterdam, 121-156.

Frazier, D. E. 1967. Recent deltaic deposits of the Mississippi River: their development and chronology. AAPG Bulletin, 51.

Gedan, K. B., Kirwan, M. L., Wolanski, E., Barbier, E. B., Silliman, B. R. 2011. The present and future role of coastal wetland vegetation in protecting shorelines: answering recent challenges to the paradigm. Climatic Change, 106, 7-29.

Georgiou, I. Y., Fitzgerald, D. M., Stone, G. W. 2005. The impact of physical processes along the Louisiana coast. J. Coastal Res., 72-89.

Higuera, P., Lara, J. L., Losada, I. J. 2014. Three-dimensional interaction of waves and porous coastal structures using OpenFOAM®. Part II: Application. Coastal Eng., 83, 259-270.

Huang, L. H., Chao, H. I. 1992. Reflection and transmission of water wave by porous breakwater. J. Waterw., Port, Coastal, Ocean Eng., 118, 437-452.

Jacobsen, N. G., Van Gent, M. R. A., Wolters, G. 2015. Numerical analysis of the interaction of irregular waves with two dimensional permeable coastal structures. Coastal Eng., 102, 13-29.

Keddy, P. 2008. Water, Earth, Fire: Louisiana's Natural Heritage. Xlibris Corporation.

Kolb, C. R., Van Lopik, J. R. 1966. Depositional environments of the Mississippi River deltaic plain—southeastern Louisiana. 17-61.

Kraus, N.C, Hanson, H., Blomgren, S. 1994. Modern functional design of groins. Proc. 24th Coastal Eng. Conf., ASCE, 1,327-1,342

Kristensen, S. E., Drønen, N., Deigaard, R., Fredsoe, J. 2013. Hybrid morphological modelling of shoreline response to a detached breakwater. Coastal Eng., 71, 13-27.

Kudella, M., Oumeraci, H., De Groot, M. B., Meijers, P. 2006. Large-Scale Experiments on Pore Pressure Generation underneath a Caisson Breakwater. Journal of Waterway, Port, Coastal and Ocean Engineering, 132, 310-324.

Louisiana Coastal Wetlands Conservation and Restoration Task Force and The Wetlands Conservation and Restoration Authority (LCWC). 1998. Coast 2050: Toward a sustainable coastal Louisiana. Louisiana Department of Natural Resources. Baton Rouge, LA

Machado, B. N., Das Neves Gomes, M., Souza, J. A., De Freitas Teixeira, P. R., Isoldi, L. A., Rocha, L. A. O., Dos Santos, E. D. 2012. Geometric Optimization of An Overtopping Wave Energy Converter for Deep Water Flow. 14th Brazilian Congress of Thermal Sciences and Engineering, Rio de Janeiro, RJ, Brazil.

Mccormick, M. E. 1993. Equilibrium shoreline response to breakwaters. J. Waterw., Port, Coastal, Ocean Eng., 119, 657-670.

McCoy, N. 2015. Functionality Evaluation of the Wave Suppressor and Sediment Collection (WSSC) System: Wave Reduction, Sediment Collection, Mathematical Modeling, and Preliminary Field Evaluation. M.S. Thesis, University of Louisiana at Lafayette.

McCoy, N., Tang, B., Besse, G., Gang, D., Hayes, D. 2015. Laboratory study of a novel marsh shoreline protection structure: Wave reduction, silt-clay soil collection, and mathematical modeling. Coastal Eng., 105, 13-20.

Meade, R. H., Parker, R. S. 1985. Sediment in rivers of the United States. US Geol. Surv. Water-Supply Paper, 2275, 49-60.

Meyer, D. L., Townsend, E. C., Thayer, G. W. 1997. Stabilization and erosion control value of oyster cultch for intertidal marsh. Restoration Ecology, 5, 93-99.

Ming, D., Chiew, Y.-M. 2000. Shoreline changes behind detached breakwater. J. Waterw., Port, Coastal, Ocean Eng., 126, 63-70.

Morang, A., Waters, J. P., Khalil, S. M. 2012. Gulf of Mexico regional sediment budget. J. Coastal Res., 14-29.

Nersesian, G. K., Kraus, N. C., Carson, F. C. Functioning of groins at Westhampton Beach, Long Island, New York. Coastal Engineering Conference, 1992. Asce American Society of Civil Engineers, 3357-3357.

Nicholls, R. J., Leatherman, S. P., Dennis, K. C., Volonte, C. R. 1995. Impacts and responses to sea-level rise: qualitative and quantitative assessments. J. Coastal Res., 26-43.

Penland, S., Ramsey, K. E. 1990. Relative sea-level rise in Louisiana and the Gulf of Mexico: 1908-1988. J. Coastal Res., 323-342.

Piazza, B. P., Banks, P. D., La Peyre, M. K. 2005. The potential for created oyster shell reefs as a sustainable shoreline protection strategy in Louisiana. Restor. Ecol., 13, 499-506.

Rosen, D. S. 1982. Sedimentological Influences of Detached Breakwaters. Coastal Eng. 1982.

Salinas, L. M., Delaune, R. D., Patrick Jr, W. H. 1986. Changes occurring along a rapidly submerging coastal area: Louisiana, USA. J. Coastal Res., 2, 269-284.

Scyphers, S. B., Powers, S. P., Heck, K. L., Byron, D. 2011. Oyster Reefs as Natural Breakwaters Mitigate Shoreline Loss and Facilitate Fisheries. PLoS ONE, 6, 1-12.

Shepard, C. C., Crain, C. M., Beck, M. W. 2011. The protective role of coastal marshes: a systematic review and meta-analysis. PloS one, 6(11), e27374.

Smith, R. D. 1993. A conceptual framework for assessing the functions of wetlands. Technical Report WRPDE-3, Vicksburg, Miss: U.S. Army Corps of Engineers, Waterways Experiment Station. 27 pp.

Tarpagkou, R., Pantokratoras, A. 2013. CFD methodology for sedimentation tanks: The effect of secondary phase on fluid phase using DPM coupled calculations. Applied Mathematical Modelling, 37(5), 3478-3494.

Thinglas, T., D. R. Kaushal. 2008a. Comparison of two and three-dimensional modelling of invert trap for sewer solid management. Elsevier: Particuology 6:176–84.

Tibbetts, J. 2006. Louisiana's Wetlands: A Lesson in Nature Appreciation. Environmental Health Perspectives, 114(1), A40–A43.

U.S. Army Corps of Engineers. 1992. Coastal Groins and Nearshore Breakwaters. Engineer Manual, No. 1110-2-1617, Washington, D.C.

Van Rijn, L.C. 1995. Sand budget and coastline changes of the central Dutch coast between Den Helder and Hoek van Holland Report H2129, Delft Hydraulics, The Netherlands.

Van Rijn, L.C. 1998. Principles of Coastal Morphology. Aqua Publications, The Netherlands.

Van Rijn, L. C. 2011. Coastal erosion and control. Ocean and Coastal Management, 54(12), 867-887.

Walker, J. H., Coleman, J. M., Roberts, H. H., Tye, R. S. 1987. Wetland loss in Louisiana. Geography Annual, 69, 189-200.

Yan, H., Kouyi, G. L., Gonzalez-Merchan, C., Becouze-Lareure, C., Sebastian, C., Barraud, S., and Bertrand-Krajewski, J. L. 2014. Computational fluid dynamics modelling of flow and particulate contaminants sedimentation in an urban stormwater detention and settling basin. Environmental Science and Pollution Research, 21(8), 5347-5356.

Yu, X. 1995. Diffraction of water waves by porous breakwaters. J. Waterw., Port, Coastal, Ocean Eng., 121, 275-282.

APPENDIX A

Modeling in Ansys FLUENT

The problem now considered is two-dimensional (2D), (figure 1). It is basically particle (sediment) transport along with waves.

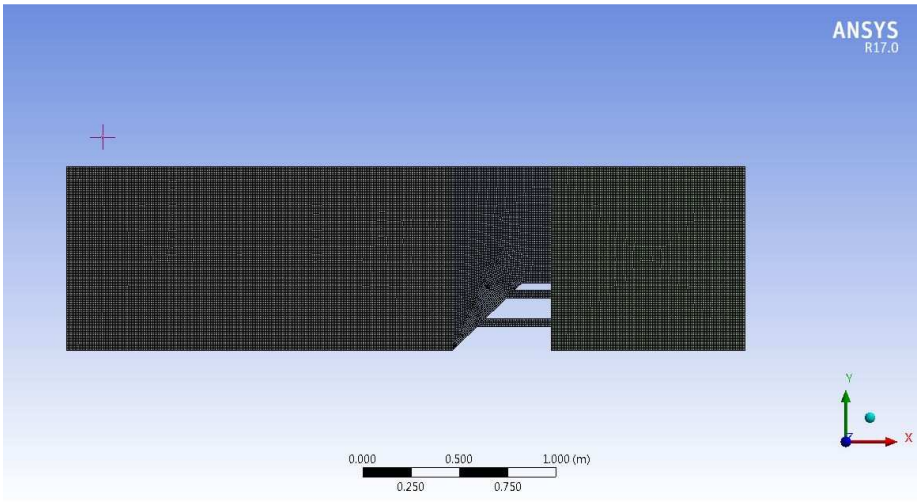

Figure 1: Geometry and problem specification

Geometry and Meshing:

This task is done every time because the research is testing different unit designs. So, every time a new geometry is tried out it has to be drawn and meshed separately. Then modeling can be performed with required conditions in Fluent. AutoCAD can also be used for drawing the units. The surfaces have to be named in the mesh so that later those can be used for simulation and generation of results. The following steps were initially followed to set up a working model for the simulation studies. Parametric values here always do not represent the exact values used in the modeling study. Modifications were made to the model setup based on study requirements.

Setup and Solution

Step 1: Mesh

The preparation of the 2D-quad mesh for this case is the first step after the geometry and meshing.

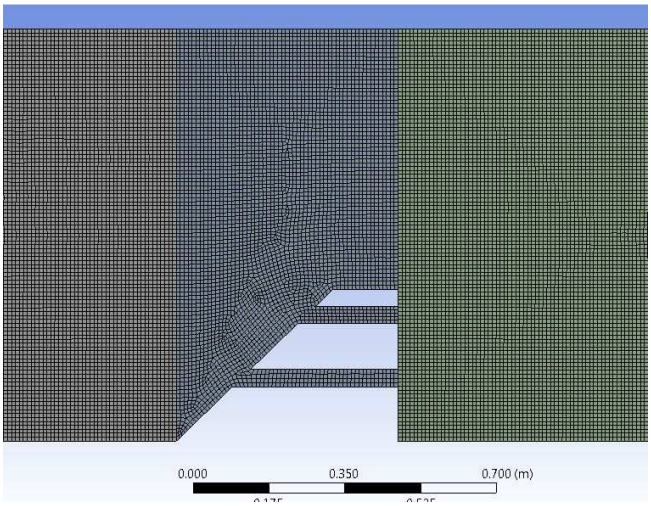

Figure 2: Meshed Geometry

The mesh size is 1 mm. It is loaded in fluent in a common way:

Command: File -> Read -> Mesh …

Step 2: General

1. Check the mesh.

   General -> Check

2. Enable the transient solver by selecting Transient from the Time list.

   General -> Transient

3. Enable Gravity -> *-9.81 in Y direction*

Step 3: Models

1. Define the multiphase model, VOF Model for this case.

   Models -> Multiphase -> Edit

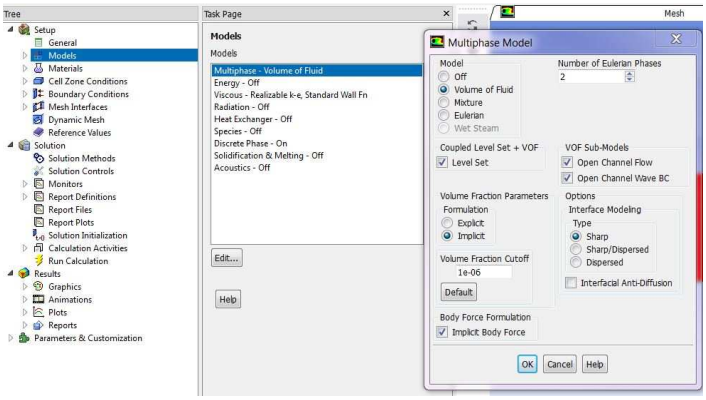

Figure 3: Model Selection

Step 4: Materials

1. Copy water-liquid (h2o<l>) from the database.

   Click the Fluent Database to open the Fluent Database Materials dialog box.

   Select water-liquid (h2o<l>) from the Fluent Fluid Materials selection list.

   Click Copy and close the Fluent Database Materials dialog box.

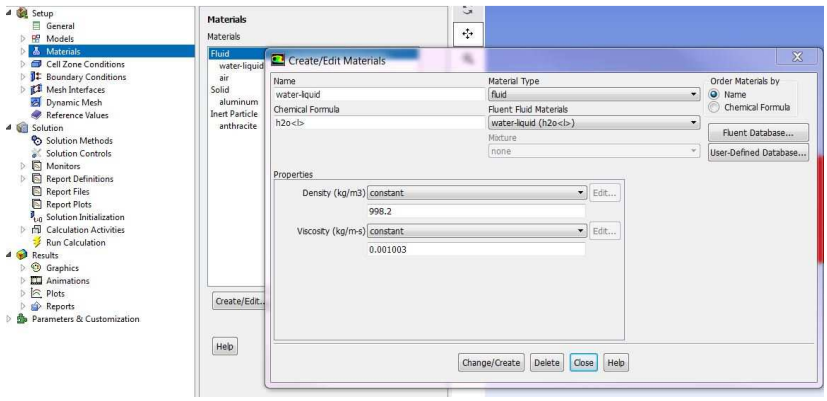

Figure 4: Defining Materials

Leave default values for Density and Viscosity.

Click Change/Create and close Create/Edit Materials dialog box.

Step 5: Phases

1. Define the primary phase

   Phases -> Primary Phase -> Edit

Enter air for Name

Select air from the phase Material drop-down list.

Click OK to close the Primary Phase dialog box.

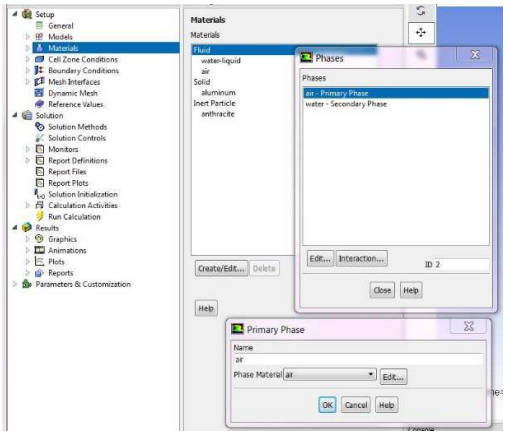

Figure 5: Defining Phases

2. Define the secondary phase

Phases -> Secondary Phase -> Edit

Enter water for Name

Select water-liquid from the phase Material drop-down list.

Click OK to close the Primary Phase dialog box.

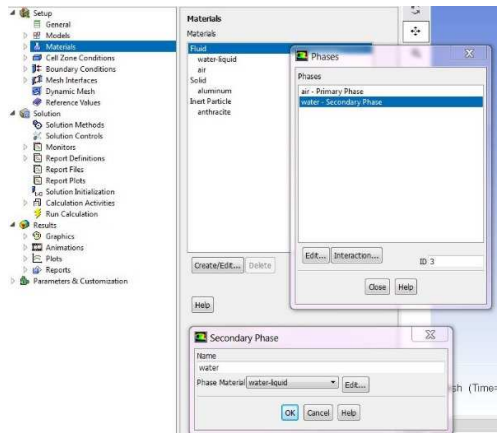

Figure 6: Naming of Phases

Step 6: Boundary Conditions

1. Set the boundary conditions for the pressure outlet

Boundary Conditions… -> movingwall (Velocity Inlet)

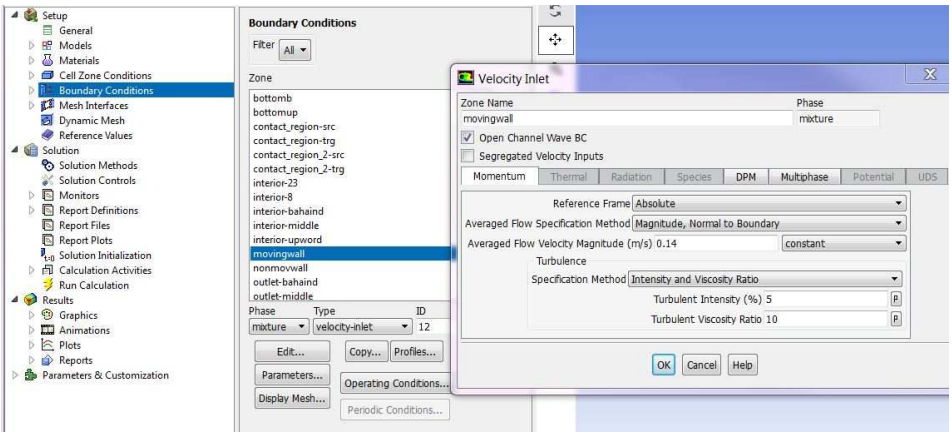

Figure 7: Defining Inlet Boundary Conditions

2. Select mixture from the Phase drop-down list and click the Edit… button to open the Velocity Inlet dialog box.
3. Edit value of 0.14 for the Velocity Magnitude.
4. Select the Multiphase from the Velocity Inlet drop-down list and click the Edit… button to open the Multiphase dialog box.
5. Enter the wave parameters as in the figure below:

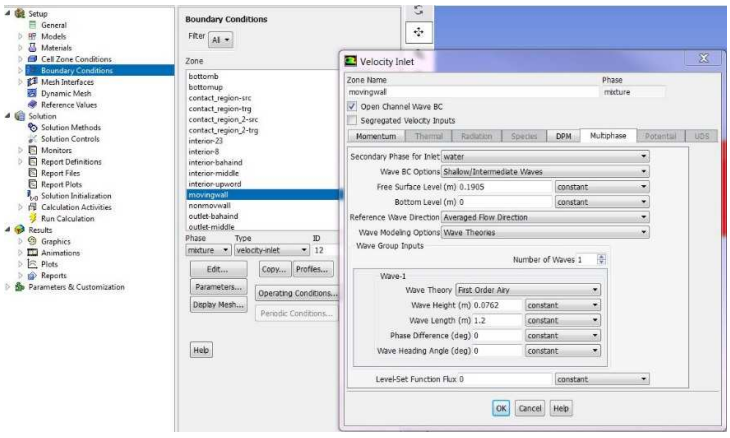

Figure 8: Wave Parameter Input

6. Click OK to close the Velocity Inlet dialog box.

7. Set the boundary conditions for the Pressure Outlet at the right side of the domain.

Boundary Conditions… -> nonmovingwall

Select mixture from the Phase drop-down list and click the Edit… button to open the Pressure-Outlet dialog box.

Write 0.1905 value for the Free Surface Level and enable Open Channel.

Click OK to close the Pressure Outlet dialog box.

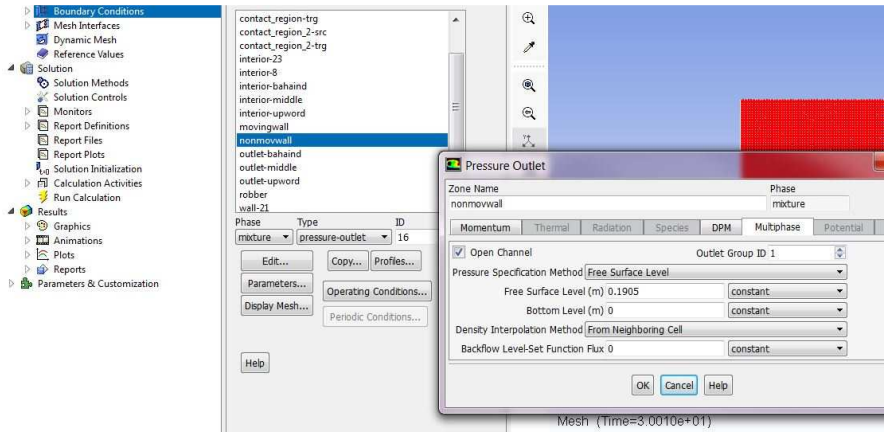

Figure 9: Defining Outlet Boundary Conditions

8. Set the boundary conditions for the other Pressure Outlets.

Boundary Conditions… -> outlet-behind, outlet-middle, and outlet-upward

Keep the default values for all Pressure Outlets.

Step 7: Operating Conditions

1. *Boundary Conditions… -> Operating Conditions*
2. Enable Gravity.
3. Enter 9.81 m/s^2 for Gravitational Acceleration in X direction

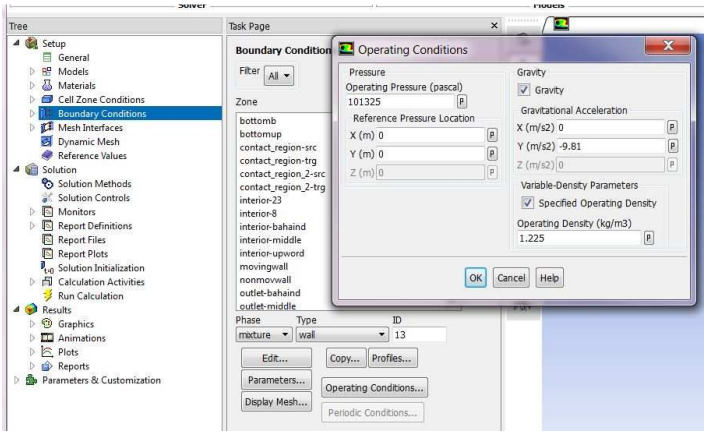

Figure 10: Defining Operating Conditions

Step 8: Solution Methods

1. Select Green-Gauss Cell-Based from the Gradient drop-down list.
2. Select Body Force Weighted from the Pressure drop-down list.
3. Select Second Order Upwind for the Momentum and First Order Upwind for Volume Fraction. Use Fist Order Implicit for Transient Formulation.

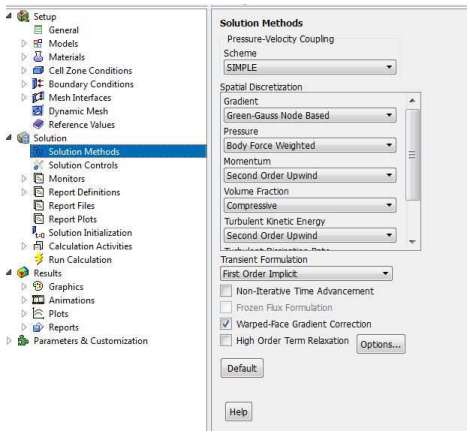

Figure 11: Solver Setting Inputs

Step 9: Solution Initialization

Solution Initialization - > Initialize.

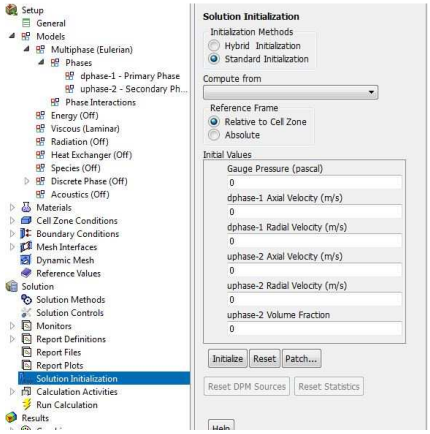

Figure 12: Solution Initialization

1. Patch a volume fraction for the u-phase
2. *Solution Initialization - > Patch...*

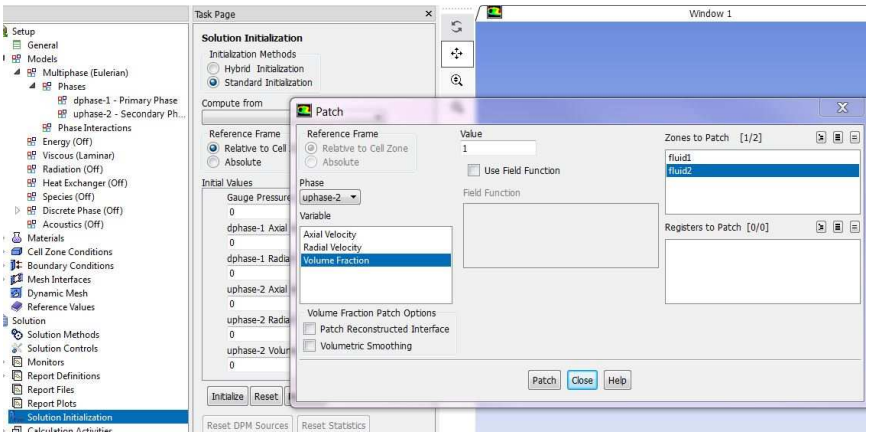

Figure 13: Solution Initialization

3. Select Volume Fraction from the Variable selection list and enter 1 for the Value and select fluid2 from the Register to Patch selection list.
4. Click Patch and close the Patch dialog box.

Step 10: Run the calculation

1. Run Calculation.
2. Enter 0.3 as the Time Step Size.
3. Enter 10000 for Number of Time Steps.
4. Enter the values for the Variable Time Step Setting as in Figure below.

5. Save the case and data files (*two-phase.cas.gz* and *two-phase.dat.gz*).

6. Click Calculate.

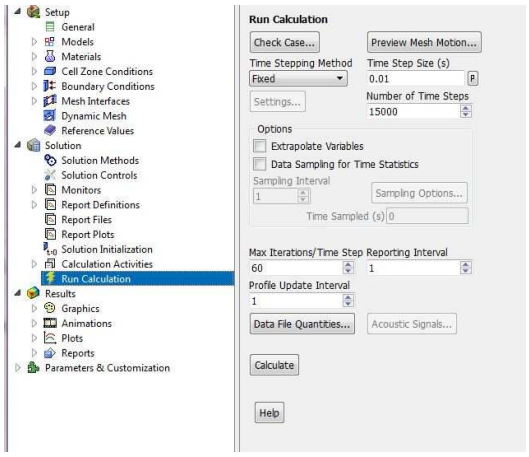

Figure 14: Running Calculation

Step 11: Post Processing

1. Read the data file for the one-time step (two-phase-1-00100.dat).

   File -> Read -> Data ...

2. Display filled contours of liquid velocity magnitude (Figure below).

   Graphics and Animations -> Contours -> Set Up ...

   Select Filed from the Options list.

   Select Phases… and dphase-1 from the Contour of the drop-down list.

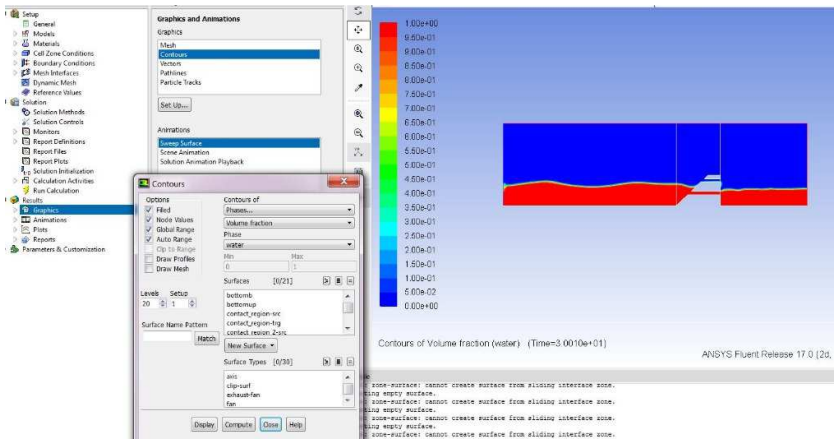

Figure 15: Post-processing of Results

Sakib, Salman. Bachelor of Science, Bangladesh University of Professionals, Fall 2014;
Master of Science, University of Louisiana at Lafayette, Summer 2017
Major: Civil Engineering
Title of Thesis: Design Optimization and Field Performance Evaluation of the Wave Suppression and Sediment Collection (WSSC) System: Computational Fluid Dynamics (CFD) Modeling, Surface Elevation Table (SET), and Marker Clay Study
Thesis Director: Dr. Daniel Gang;
Pages in Thesis: 87; Words in Abstract: 303

ABSTRACT

Coastal erosion is an issue of concern for Louisiana, in the United States, and for all other coastal communities in the world. Among many coastal protection and restoration technologies, shoreline protection structures focus on wave reductions to prevent waves from hitting the coastal landforms directly. A novel technology called the Wave Suppression and Sediment Collection (WSSC) system focuses on solving the limitations of conventional shoreline protection structures regarding mobility, constructability, and sustainability. The primary goals of this study are to optimize the WSSC units for wave reduction and sediment transport and to verify the performance of this technology in an actual field environment. Computational Fluid Dynamics (CFD) simulations were carried out to optimize the designs of the units in terms of pipe diameters and face slope. Results have indicated that increasing pipe diameters decreases wave reduction and increases sediment transport ability of the units. Further, it was found that increasing the face slope decreases the wave reduction ability; however, no effect was found on the sediment transport efficiency. Parametric optimization suggested that a porosity (open-to-total area ratio) of 30% should yield satisfactory wave reduction and balanced sediment transport by the units. For better output from the units, the designs should be modified according to site-specific requirements. Field site investigations involved Surface Elevation Table (SET) surveying and marker clay experiments. SET surveys showed significant sediment accumulation over eleven months behind the units.

Also, no significant change was observed at the control site over three months, which proves the effectiveness of the technology in stopping erosion and facilitating land building. Marker clay experiments validated the SET measurements and proved that there was a significant amount of sediment deposition over the white Feldspar clay layer over six months. This strengthens the conclusion that the WSSC units can be used successfully in a Louisiana marsh environment to battle coastal erosion and land loss.

BIOGRAPHICAL SKETCH

Salman Sakib was born in the District of Naogaon, Bangladesh on August 22, 1992. He obtained his Bachelor of Science in civil engineering from Bangladesh University of Professionals (BUP) in 2014. He joined the University of Louisiana at Lafayette as a graduate research assistant in the Civil Engineering Department to pursue a Master of Science in civil engineering with environmental engineering concentration. He has authored and co-authored papers relating to environmental and coastal engineering topics. He completed his Master of Science degree in Summer 2017 and plans to work as a researcher to tackle environmental engineering issues.